N88-17597

BOUNDARY-LAYER AND WAKE MEASUREMENTS ON A SWEPT, CIRCULATION-CONTROL WING

Frank W. Spaid
McDonnell Douglas Research Laboratories

Earl R. Keener
NASA Ames Research Center

SUMMARY

Wind-tunnel measurements of boundary-layer and wake velocity profiles and surface static-pressure distributions are presented for a swept, circulation-control wing. The model is an aspect-ratio-four semispan wing mounted on the tunnel side wall at a sweep angle of 45°. The 25.4-cm constant-chord airfoil is a 20% ellipse, modified with circular leading and trailing edges of 4% radius. This configuration does not represent a specific shape from current vehicle design concepts which are being developed. A full-span, tangential, rearward-blowing, circulation-control slot is located ahead of the trailing edge on the upper surface. Flow surveys were obtained at mid-semispan at freestream Mach numbers of 0.425 and 0.70, Reynolds numbers based on streamwise chord of 2.3×10^6 and 3.2×10^6, angles of attack of 0° and 5°, and jet stagnation to freestream static-pressure ratios of 1.0 to 2.2. Boundary-layer profiles measured on the forward portions of the wing's upper and lower surfaces are approximately streamwise and two-dimensional. The flow in the vicinity of the jet exit and in the near wake is highly three-dimensional. The jet flow near the slot on the Coanda surface is directed normal to the slot, or 45° inboard. All near-wake surveys show large outboard flows at the center of the wake. At Mach 0.425 and a 5° angle of attack, a range of jet blowing rates was found for which an abrupt transition from incipient separation to attached flow occurs in the boundary layer upstream of the slot. The variation in the lower-surface separation location with blowing rate was determined from boundary-layer measurements at Mach 0.425.

*This research was conducted under the McDonnell Douglas Independent Research and Development Program in cooperation with the NASA Ames Research Center.

NOMENCLATURE

$b/2$ semispan

c streamwise wing chord

c_ℓ section lift coefficient

C_f local skin-friction coefficient, τ_w/q_e

C_p pressure coefficient, $(p-p_\infty)/q_\infty$

C_μ jet momentum coefficient, $m_j V_j/q_\infty S$

m_j jet mass-flow rate

M Mach number

p pressure

q dynamic pressure, $(1/2)\rho u^2$

Re_c Reynolds number based on chord

S wing area, defined as the product of the slot length and the wing chord measured normal to the section generators

u velocity magnitude

u_s component of velocity parallel to flow direction at edge of boundary layer

u_τ shear velocity, $\sqrt{\tau_w/\rho_w}$

V_j computed jet velocity assuming isentropic expansion from jet stagnation pressure to p_∞

x coordinate measured parallel to freestream direction

y spanwise coordinate

z coordinate normal to wing plane

z^+ law-of-the-wall coordinate, $(zu_\tau)/\nu_w$

α wing angle of attack

β yaw-plane flow direction angle, positive outboard

δ_1^* streamwise displacement thickness, $\int_0^\delta \left(1 - \frac{\rho u_s}{\rho_e u_e}\right) dz$

ν kinematic viscosity

ρ density

σ pitch-plane flow direction angle, positive upward

τ_w wall shear stress

Subscripts

e conditions at edge of boundary layer

j jet parameter

w conditions at surface

∞ freestream conditions

INTRODUCTION

There are several ways to control the aerodynamic circulation of wings and thus, the amount of lift. One type of circulation control that is currently under investigation is tangential blowing from a slot located ahead of a rounded trailing edge. The tendency of the flow to adhere to the trailing-edge surface is known as the Coanda effect. The deflected flow can increase the lift of a wing section to several times that obtained by the conventional method of increasing the angle of attack. Wood and Nielsen (1985) present a summary of circulation-control research.

A cooperative investigation of the boundary layer and wake of a swept, circulation-control wing was recently conducted by NASA Ames Research Center and McDonnell Douglas Research Laboratories in the Ames Six- by Six-Foot Transonic Wind Tunnel. The test was conducted in support of the NASA X-Wing stopped-rotor research vehicle, which is designed to cruise at high speed with the rotor stopped in the X-wing configuration (Wood and Nielsen, 1985). The model is an aspect-ratio-four semispan wing mounted on the side wall. The 25.4-cm constant-chord airfoil is a 20% ellipse, modified with circular leading and trailing edges. This generic configuration does not represent a specific shape from current vehicle design concepts which are being developed. A full-span, tangential, rearward-blowing circulation-control slot is located ahead of the trailing edge on the upper surface. The wing was tested at Mach numbers from 0.3 to 0.75 at sweep angles of 0° and 45° with internal-to-external pressure ratios of 1.0 to 3.0. Lift and pitching-moment coefficients were obtained from measured pressure distributions. Surface-flow patterns were photographed using the oil-streak flow-visualization method.

This paper presents the results of the boundary-layer and wake measurements at Mach numbers of 0.425 and 0.70 at 45° sweep angle. The pressure measurements and oil-flow photographs are presented by Keener et al. (1986).

TEST FACILITY

The Ames Six- by Six-Foot Transonic/Supersonic Wind Tunnel was chosen because the allowable model size and the tunnel operational characteristics are suitable for boundary-layer research. The tunnel is a variable-pressure, continuous-flow facility. The nozzle leading to the test section is of the asymmetric sliding-block type that permits a continuous variation of Mach number from 0.25 to 2.3. The test section has a slotted floor and ceiling with 6% porosity and provisions for boundary-layer removal. The turbulence level is measured to be about 1.5% rms of the freestream velocity.

MODEL

Details of the model design are given by Keener et al. (1986). The model is a semispan wing incorporating circulation control by tangential blowing from a spanwise slot located ahead of a rounded trailing edge. The model was mounted on the sidewall of the tunnel on a turntable that could be manually rotated through a ±5° range in angle of attack. The wing-root mounting structure is covered by a fairing. Figure 1 is a sketch of the model installation in the tunnel showing the zero- and 45° sweep positions. The resulting aspect ratios are 4.0 and 1.85, respectively, based on the normal component of the exposed span. The sketch also shows the position of the boundary-layer traversing unit, which was mounted on a bracket attached to the tunnel center-body support. Figure 2 shows views of the model in the 45° sweep position and the boundary-layer traversing unit.

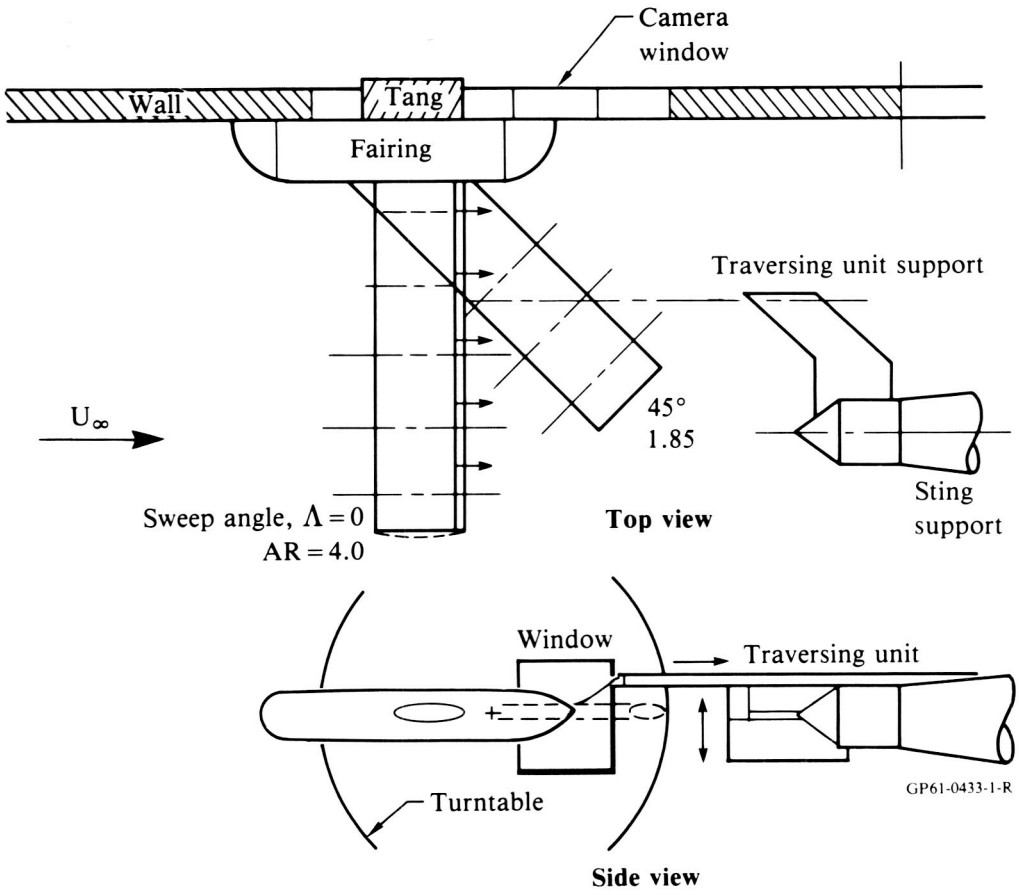

Figure 1. Sketch of model and traversing unit installation.

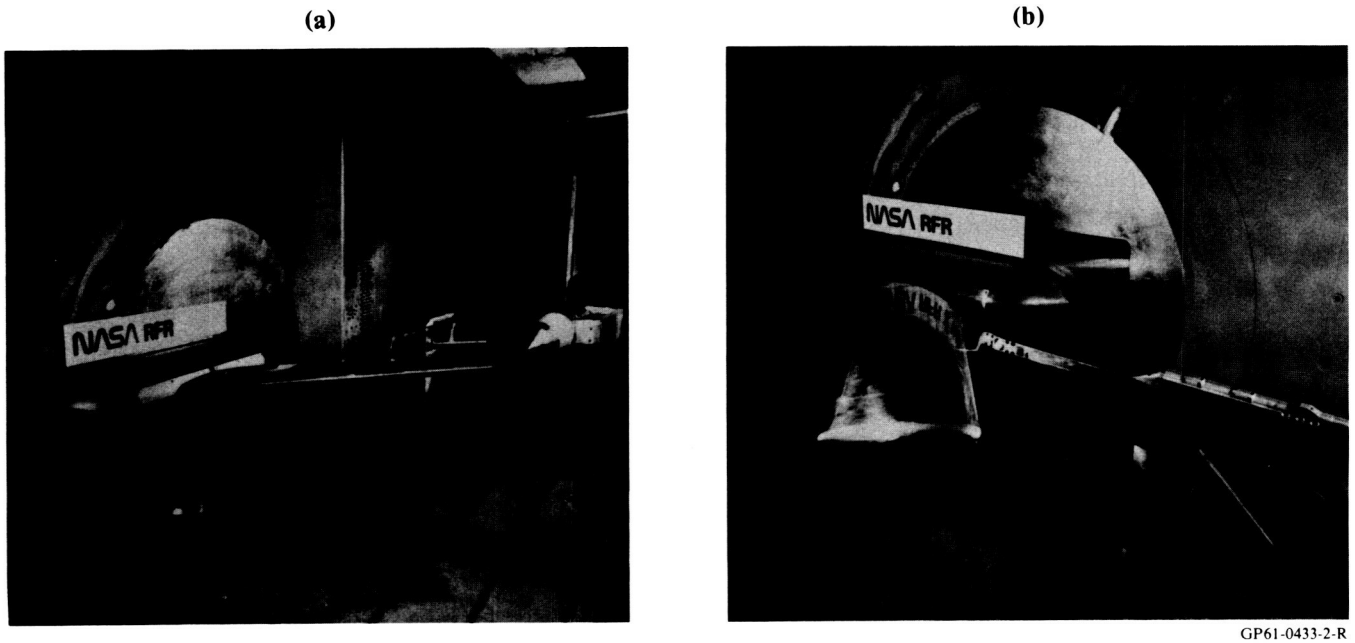

Figure 2. Wing model at a sweep angle of 45° and probe traversing unit.

The wing has a 20% elliptical section and a 25.4-cm constant chord, modified with circular leading and trailing edges of 4% radius (figure 3). A full-span, tangential, rearward-blowing, circulation-control slot, with a nominal slot height of 0.0020 chord and a trailing-edge thickness of 0.0008 chord, was incorporated ahead of the trailing edge on the upper surface.

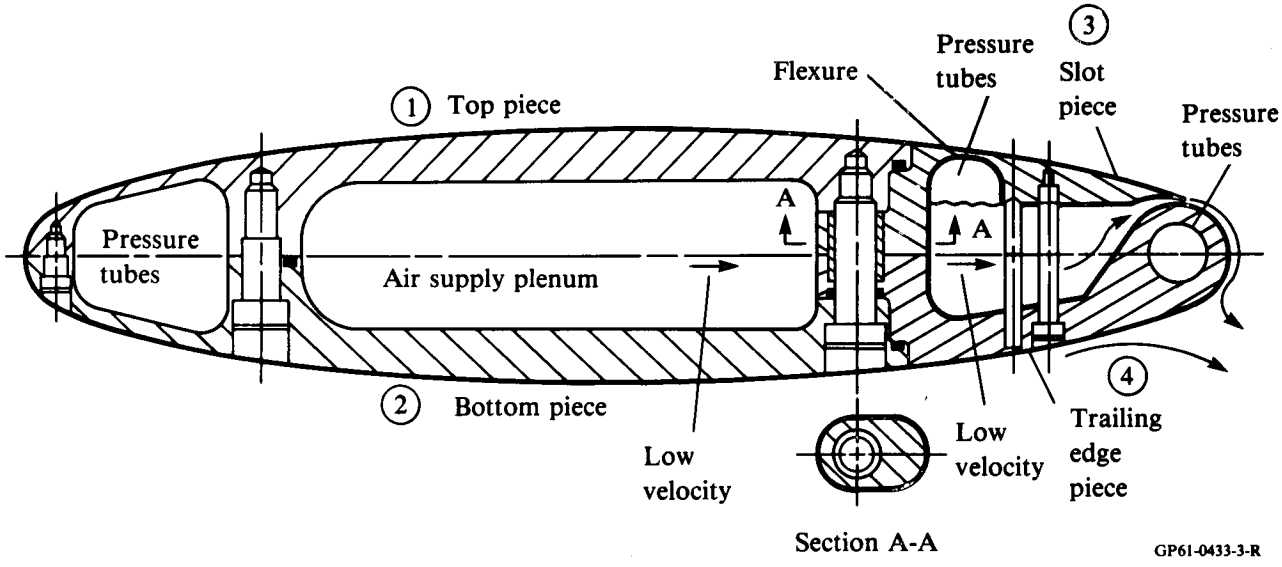

Figure 3. Sketch of wing section showing four-piece construction, bolts, set screw, and adjusting screw for slot height.

Design suggestions based on experience with previous circulation-control tests were contributed by N. Wood, Stanford Institute for Aeronautics and Aeroacoustics, and by E. Rogers and J. Abramson, David W. Taylor Naval Ship Research and Development Center. Publications from their research are discussed in the review paper by Wood and Nielsen (1985). The model design follows closely the design concepts of Wood and Conlon (1983), and Wood and Sanderfer (1987).

The model was designed in four parts (figure 3), split along the plane of symmetry. The center of the model contains an internal plenum, which was connected to the external air supply at the wing root through the sidewall of the tunnel. The air supply was provided from the tunnel 550-kPa dry-air sphere. The air flow was controlled by a regulator to set the total pressure in the wing plenum. The design of the trailing-edge Coanda surface and slot is described by Keener et al. (1986).

INSTRUMENTATION AND DATA REDUCTION

Details of the pressure instrumentation are given by Keener et al. (1986). The pressure instrumentation consisted of 252 orifices on the wing, installed at five spanwise stations (rows 1 to 5: $2y/b = 0.1$, 0.3, 0.5, 0.7, and 0.9, based on the exposed span at zero sweep) and one row of orifices at the midspan of the wing-root fairing (figure 4). More orifices were placed at row 4, $2y/b = 0.7$, especially over

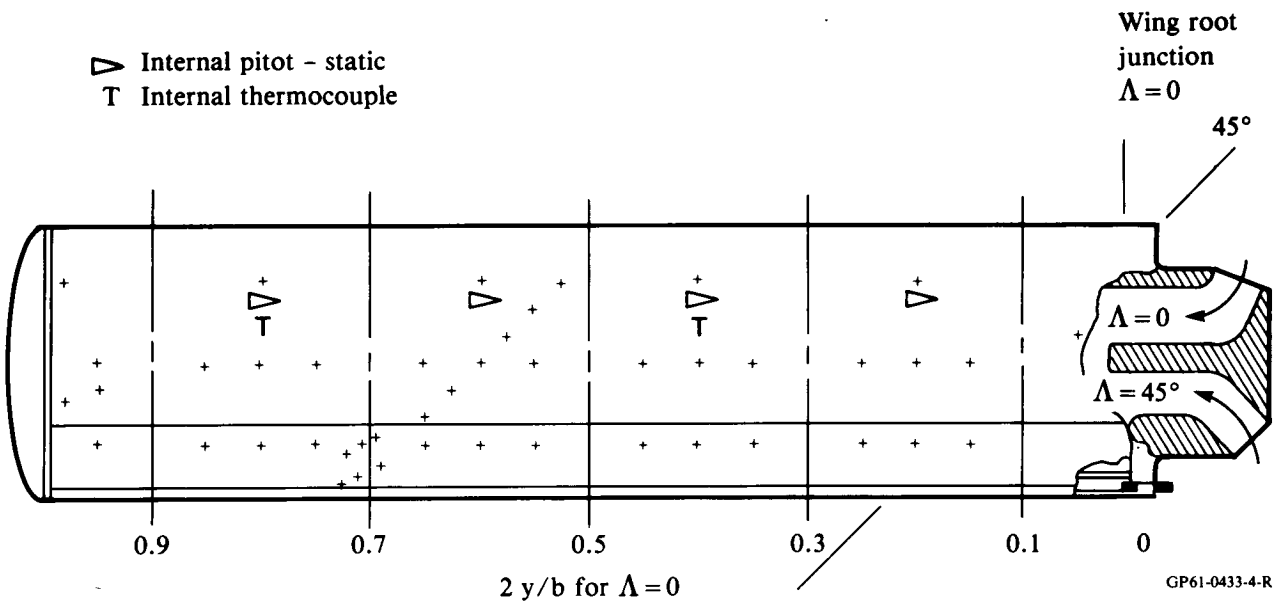

Figure 4. Layout of wing static-pressure orifices.

the trailing edge, in order to obtain more detail at one row. Additional orifices were placed at row 6 at a 45° angle between rows 3 and 4 (2y/b = 0.5 and 0.7) to assist in the analysis of the pressures at a sweep angle of 45° and to provide a row of orifices near the location of the upper-surface boundary-layer measurements.

The surface static pressures were measured with electronically actuated pressure-scanning valves containing pressure transducers that were connected to an automatic data-recording system. The self-calibrating feature of the scanning valves provided an accuracy of about 0.25% of full scale of the ±86.2-kPa transducers, providing an accuracy in pressure coefficient of approximately ±0.01. Tunnel test conditions were measured with precision pressure transducers, resulting in a Mach number accuracy of about ±0.002. Tunnel static pressure was measured on the tunnel wall 10 wing-chord lengths ahead of the wing-root leading edge. Angle of attack was set manually by rotating the wall turntable and setting the angle with an inclinometer with an accuracy of ±0.03°.

Static-pressure measurements were reduced to standard pressure coefficients by use of the tunnel conditions which were measured at the beginning of each data set. The data were recorded, processed, and plotted by the tunnel data-acquisition system. Pressure coefficients for each spanwise station were numerically integrated by the trapezoidal rule to determine wing-section normal-force and pitching-moment coefficients. Wing-panel normal-force, pitching-moment, and bending-moment coefficients were determined by Simpson's-rule numerical integration of the span-load distributions. Jet total mass flow was determined from a calibrated orifice plate mounted in the air supply line. The jet velocity was calculated using the freestream static pressure as the jet-exhaust pressure.

The traversing unit shown in figures 1 and 2 contains stepper motors that allow remote movement of the probe tip in the streamwise and vertical directions; the probe location is determined with the aid of encoders. Streamwise position resolution is 0.087 mm per encoder pulse, and vertical resolution is 0.0052 mm per encoder pulse. A

microcomputer-based probe control system allows manual operation of the unit and also provides an automatic mode in which data are obtained in a preprogrammed sequence of probe movements and data-acquisition cycles. The wing surface was located by electrical contact between the wing and the probe tip at the beginning of a boundary-layer survey. The probe tips used for most boundary-layer surveys are small, flattened, three-hole probes; the wake surveys and some wall-jet surveys (flowfield surveys above the Coanda surface) were made with a small five-hole probe. Sketches of the probes are shown in figure 5. The tip of the five-hole probe was inclined upward 15°, to reduce its flow interference in the wake downwash. To reduce flow interference and minimize flow angle and stagnation-pressure measurement errors, the three-hole probes were adjusted in pitch angle so that the tips were nearly parallel to the wing surface. The probes are similar to those described by Dudzinski and Krause (1969).

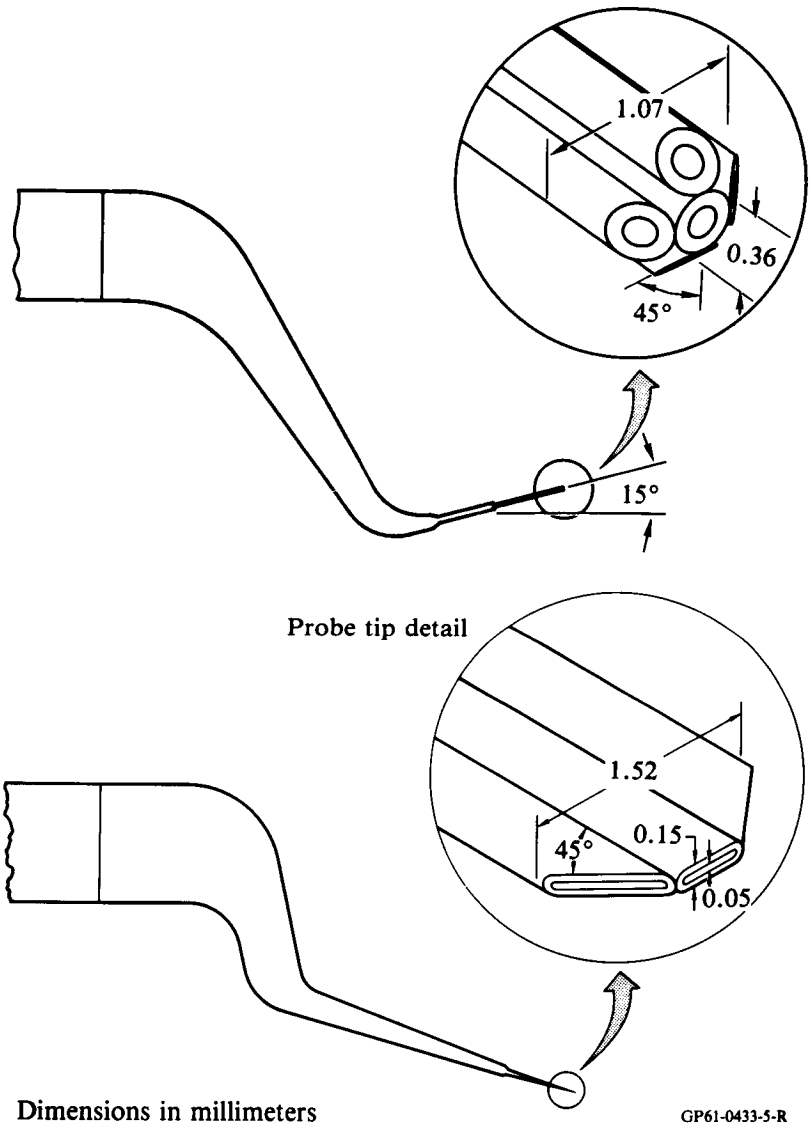

Figure 5. Three- and five-hole probes.

A pressure transducer was connected to each probe orifice through a fluid switch. Data for a two-point calibration of each transducer were obtained by cycling the switch at the beginning and end of each boundary-layer survey. The accuracy of individual probe pressure measurements was estimated to be ±0.15 kPa, corresponding to approximately ±1.3% and ±0.6% of freestream dynamic pressure at Mach 0.425 and 0.70, respectively. Probe pressure errors were estimated by root-mean-square combination of estimated errors resulting from uncertainties in reference and calibration pressures, nonlinearity and hysteresis of the transducers, and the recording resolution of the microcomputer.

Probe calibrations were performed in a free-jet calibration facility, following the procedures outlined by Dudzinski and Krause (1969). Probe-angle-measurement accuracy was ±0.1°, and accuracy of pressure measurement was estimated to be ±0.15 kPa, as before. Calibrations were performed at six Mach numbers, ranging from 0.25 to 1.0. Three-hole-probe calibrations were performed over an angle range of ±40° in the yaw plane, and five-hole-probe calibrations were performed over a range of ±40° in the pitch plane and +60° to -40° in the yaw plane, relative to the probe tip. Probe readings corresponding to the freestream flow direction were determined in the wind tunnel by taking probe data at a position approximately 0.7 m above the wing, with the wing at 0° angle of attack, and a low jet-blowing rate, to stabilize the wing wake. In reducing the three-hole-probe data, stagnation-pressure corrections and angles were determined from the probe data alone, since this can be done accurately without knowledge of the local static pressure. Mach number and velocity profiles were computed from the three-hole-probe data with the aid of the local static pressure interpolated from the surface-orifice data. Pitot pressure, flow angles, and static pressure were determined from the five-hole-probe measurements. A search and interpolation procedure, in which the local Mach number was explicitly included as an independent variable, was performed on the entire probe-calibration data base.

TEST CONDITIONS AND PROCEDURES

The wing pressures were first measured without boundary-layer trips at $M_\infty = 0.70$ at zero sweep. Next, boundary-layer trips were installed on the wing by use of sifted glass spherules at 9% chord. Sublimation flow-visualization tests were made at a Mach number of 0.70 to verify that the estimated trip size of 0.23-mm diameter was adequate to cause transition. When the wing was swept to 45°, a sublimation test verified that the trips were also effective at this angle.

Flow surveys were obtained at freestream Mach numbers, M_∞, of 0.425 and 0.70, Reynolds numbers based on streamwise chord, Re_c, of 2.3×10^6 and 3.2×10^6, angles of attack, α, of 0° and 5°, and ratios of jet stagnation to freestream static pressure, p_j/p_∞, of 1.0 to 2.2. The Mach numbers 0.425 and 0.70 correspond to the Mach numbers 0.30 and 0.50 at zero sweep, determined from simple sweep theory, $M_\infty/\cos 45°$. Performance data corresponding to both the swept and unswept conditions are presented by Keener et al. (1986). Boundary-layer surveys were made at one span station starting at about 20% chord at static-pressure orifice row 3, back to near the trailing edge outboard of row 4, on both upper and lower surfaces (figure 4). Wake surveys were obtained in a region 1% to 30% chord downstream of the trailing edge.

Oil-flow-visualization tests were made at both sweep angles at several Mach numbers to assist the analysis of the pressure and boundary-layer measurements (Keener et al, 1986).

RESULTS AND DISCUSSION

Three static-pressure distributions corresponding to test conditions for which probe data were obtained are shown in figure 6. The upper-surface data were obtained from the diagonal row of orifices located at the spanwise survey station, and the lower-surface data were interpolated to that station from the adjacent chordwise orifices. Blowing rates are indicated both by p_j/p_∞, and by the momentum coefficient, C_μ, the jet momentum flux normalized by the freestream dynamic pressure and the wing area. The corresponding section lift coefficient, c_ℓ, is also shown. Pressure distributions corresponding to the two values of blowing are characterized by weak suction peaks at the leading edge, near-zero pressure gradients at mid-chord, and large suction peaks on the upper surface downstream of the jet. The flow is locally supersonic in this region at the higher blowing rate; the minimum value of C_p is -4.75 (not shown).

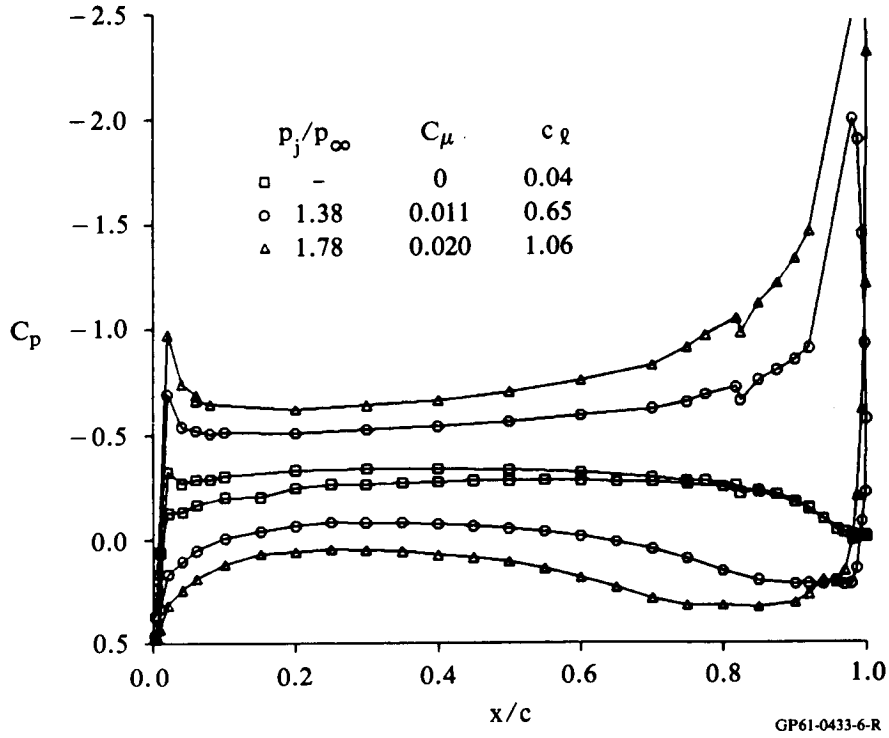

Figure 6. Wing static-pressure distributions at mid-semispan; $M_\infty = 0.425$, $Re_c = 2.27 \times 10^6$, $\alpha = 0°$.

Figures 7 and 8 are composite views in the streamwise section plane of the aft portion of the model, including the slot inlet, and the surrounding flowfields. This style of presentation is used in several of the subsequent figures to help clarify the qualitative features of these complex three-dimensional flows. The velocity vectors are projections in the streamwise plane, and the vector labeled u_∞ in the upper left corner of both figures corresponds to the freestream velocity. The boundary-layer profiles were obtained with a three-hole probe, and the vectors are drawn parallel to the local surface. The wake profiles and the wall-jet profile (the flow survey above the Coanda surface downstream of the jet exit station in figure 8) were obtained with a five-hole probe, and are drawn at the measured inclination angle.

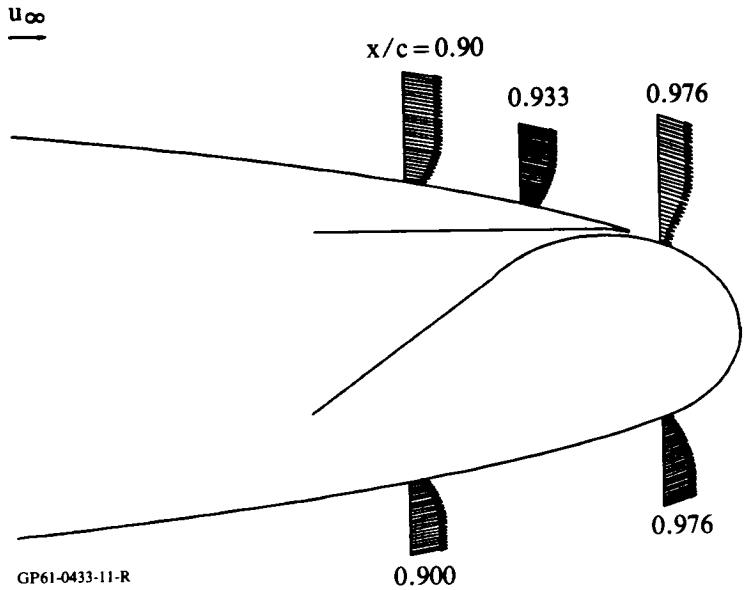

Figure 7. Velocity components in streamwise section plane; $M_\infty = 0.425$, $\alpha = 0°$, no blowing.

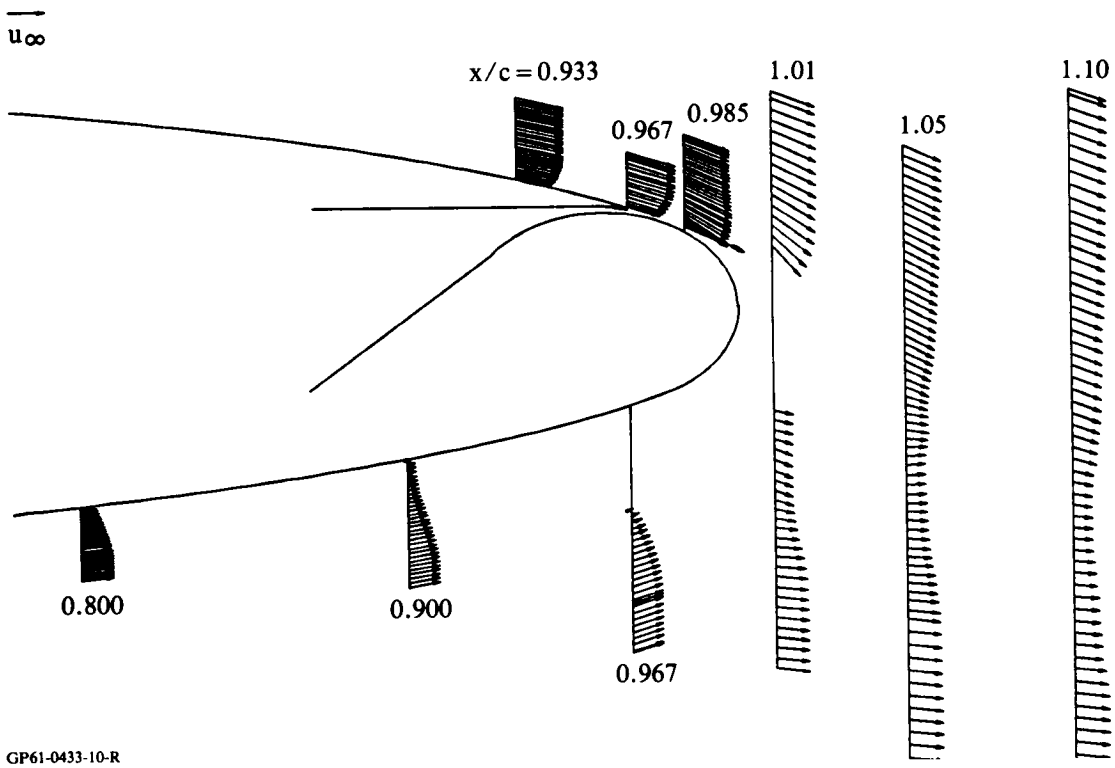

Figure 8. Velocity components in streamwise section plane; $M_\infty = 0.425$, $\alpha = 0°$, $p_j/p_\infty = 1.4$.

The data of figure 7 correspond to $M_\infty = 0.425$, $\alpha = 0°$, and no blowing. No wake data were obtained at this test condition. The boundary-layer profiles show approximately symmetrical flow, as expected, with separation apparently occurring slightly downstream of the last measuring station (x/c = 0.976) on both the upper and lower surfaces.

Figure 8 is a composite view corresponding to $M_\infty = 0.425$, $\alpha = 0°$, and $p_j/p_\infty = 1.4$, the baseline test condition selected for flowfield surveys in this investigation. The characteristics of this flowfield are in sharp contrast to data corresponding to no blowing presented in the preceding figure. The boundary-layer profiles on the upper surface upstream of the slot and at the slot lip (x/c = 0.967) are full, showing the effect of entrainment by the jet. The jet is evident in the profile obtained at x/c = 0.985. A separated region is indicated by the lower-surface boundary-layer profiles. Significant variations in pitch-plane inclination angles are present in the wake profiles; the gradients decrease with increasing x/c. The gap in the wake profile at x/c = 1.01 is a region where the flow direction exceeded the probe calibration range. The upper portion of the wake nearest the trailing edge is characterized by large negative values of the pitch-plane angle. Below the trailing edge, the pitch-plane angles are still negative, but are smaller in magnitude. Large cross-stream velocity components are present in this flowfield; the cross-stream flow is shown in subsequent figures.

Figures 9-11 present conventional velocity-magnitude and flow-angularity profiles for each of the locations surveyed at the baseline test condition of figure 8; the boundary-layer and wall-jet data of figures 9 and 10 were obtained with a three-hole probe, and the wake data of figure 11 were obtained with a five-hole probe. Figure 9a

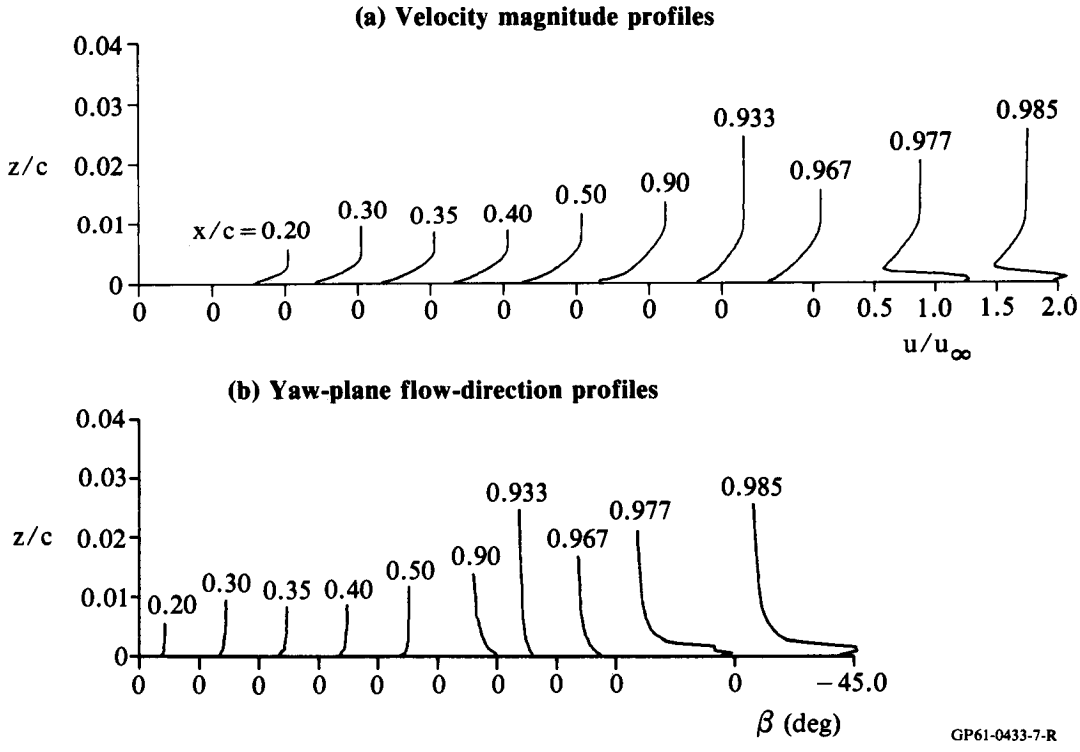

Figure 9. Upper-surface boundary-layer profiles; $M_\infty = 0.425$, $\alpha = 0°$, $p_j/p_\infty = 1.4$.

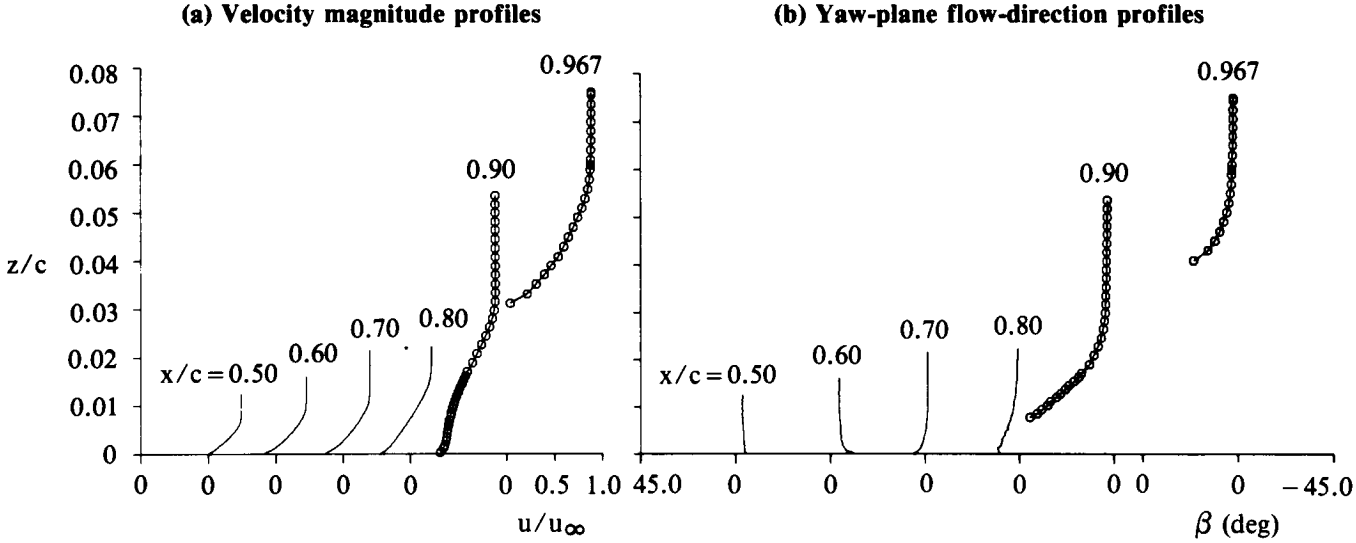

Figure 10. Lower-surface boundary-layer profiles; $M_\infty = 0.425$, $\alpha = 0°$, $p_j/p_\infty = 1.4$

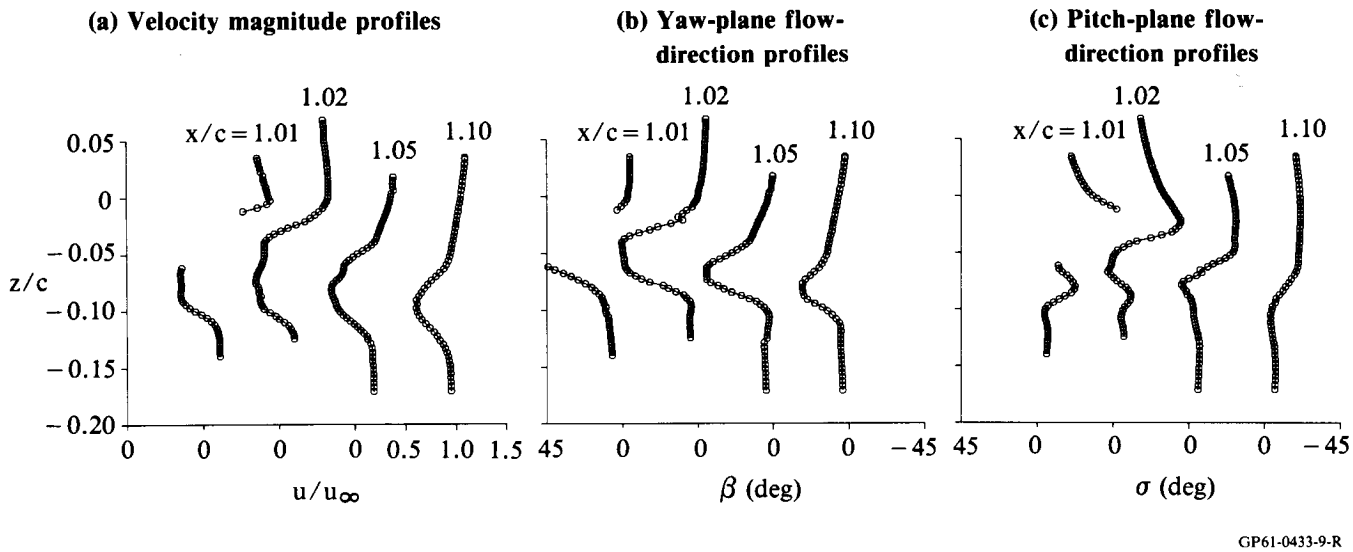

Figure 11. Wake profiles; $M_\infty = 0.425$, $\alpha = 0°$, $p_j/p_\infty = 1.4$.

gives u/u_∞, the velocity magnitude normalized by the freestream velocity, plotted against z/c, the distance from the surface normalized by the streamwise chord, for each of the upper-surface survey stations, $0.2 \leq x/c \leq 0.985$. The distance from the surface, z, is measured normal to the tunnel axis, which is also normal to the mean plane of the wing at $\alpha = 0°$. Corresponding profiles of yaw-plane flow angle, β, are shown in figure 9b (outboard flow is defined as positive β). Because of the small scale of the plots in figure 9 and in some of the subsequent figures, individual plotting symbols are not used. Approximately 40 points were obtained for each of the profiles of figure 9. The boundary-layer thickness does not increase appreciably from mid-chord to the slot station. The profiles of β upstream of the slot indicate that the flow was approximately colinear, with a mean inboard inclination which increases with increasing downstream distance. Both the thin, full character of the velocity

magnitude profiles near the slot station and the inboard values of β imply strong entrainment by the jet. The two wall-jet profiles show that the jet is directed normal to the slot (β ≈ -45°). The corresponding lower-surface profiles are shown in figure 10, beginning at x/c = 0.5. The profiles for 0.5 ≤ x/c ≤ 0.7 are full, and the flow is approximately streamwise. Downstream of x/c = 0.7, the boundary-layer growth is rapid; at x/c = 0.9 the flow is near separation. In the inner region of the profile at x/c = 0.967, the probe pressures are approximately equal to the local static pressure, indicating reverse flow, and no data are plotted. Measured values of β become increasingly outboard with decreasing distance from the surface in the two downstream profiles. Near the surface at x/c = 0.9, the probe pressure-differences are too small to allow accurate determination of β; thus, the last few points on the flow-angle profile are omitted.

Velocity magnitude, β, and pitch-plane flow-angle (σ) profiles are presented in figure 11 for four wake survey stations (upward flow is defined as positive σ). The origin of the z-coordinate for the wake profiles is the upper lip of the slot. The upper and lower portions of each profile include regions of constant stagnation pressure, indicating that the flow nonuniformities result from both inviscid and viscous effects. The upper edge of the wake near the trailing edge is characterized by high velocity magnitudes, large downwash, and nearly streamwise flow in the yaw plane; the lower edge has lower velocity magnitudes and is more nearly streamwise in both planes. The flow in the central portion of the wake is predominantly outboard, despite the fact that jet, which is strong enough to control the wing circulation, is directed 45° inboard. At x/c = 1.02, the flow at the center of the wake is approximately parallel to the trailing edge. The qualitative behavior of the flow in the gap at x/c = 1.01 is consistent with these trends; the signs of the flow angles can be determined from the signs of the appropriate probe-pressure differences even when the probe calibration range is exceeded. Apparently, the flow in the viscous central wake is dominated by the outboard flow in the separated region on the lower surface.

An illustration of the influence of the jet on the flow immediately downstream of the slot is shown in figure 12, where three-dimensional velocity-vector profiles on the Coanda surface, 1% chord downstream of the slot, are compared with and without jet flow. These are three-dimensional vector plots viewed from a point above and outboard

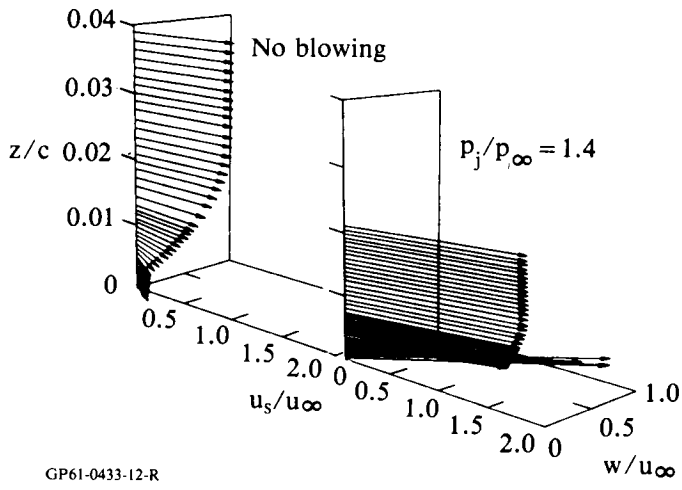

Figure 12. Velocity vector profiles; $M_\infty = 0.425$, $\alpha = 0°$, $x/c = 0.976$.

of the measuring station. The profiles were obtained with the three-hole probe and the vectors are drawn parallel to the horizontal plane of the figure. The sharp distinction between the jet flow and the remnant of the approaching boundary layer is apparent in the wall-jet profile. The outboard rotation of the velocity vectors with decreasing distance from the surface is less obvious for the no-blowing case, but the qualitative differences between the two profiles are clear. The flow near the wall for the no-blowing case corresponds to the previously mentioned situation in which the probe-pressure differences were too small to allow accurate determination of β. In this instance, values of β were extrapolated from above.

Close-ups of wall-jet and wake profiles corresponding to the baseline test condition are presented in figures 13-15. These data were obtained with the five-hole probe and are presented in the form of streamwise velocity components, cross-stream velocity components (velocity components lying in a plane normal to the freestream velocity vector) and static-pressure distributions. The profiles of figures 13-15 correspond to x/c = 0.984, 1.02, and 1.10. The streamwise profiles at x/c = 0.984 and 1.10 are also shown in figure 8. The velocity vectors are plotted to the same scale in figures 13-15, but differences in the mean value and range of variation in static pressure among the profiles required significant changes in the C_p scale.

The five-hole probe is too large to resolve the flowfield features accurately near the Coanda surface. In reducing the data shown in figure 13 corresponding to $0 \leq z/c \leq 0.0035$, the static pressure was assumed to be the value measured at the surface, the stagnation pressure was assumed to be the maximum of the values measured by the probe orifices, and the pitch-plane flow direction was assumed to be parallel to the local surface.

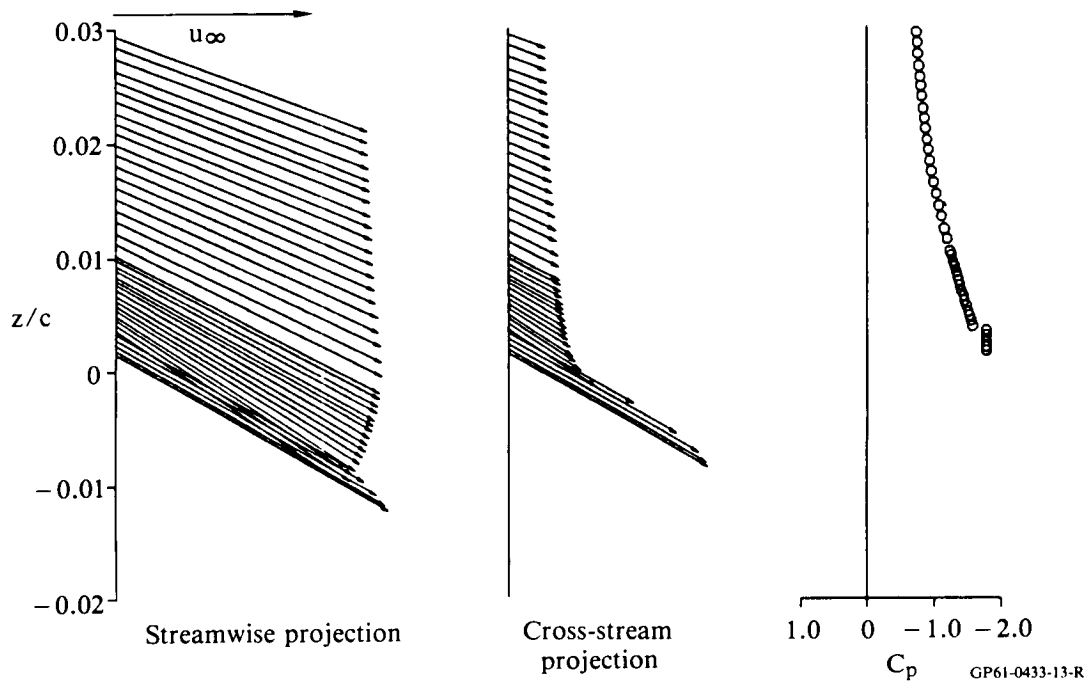

Figure 13. Wall-jet velocity and static-pressure profiles; $M_\infty = 0.425$, $\alpha = 0°$, $p_j/p_\infty = 1.4$, $x/c = 0.984$.

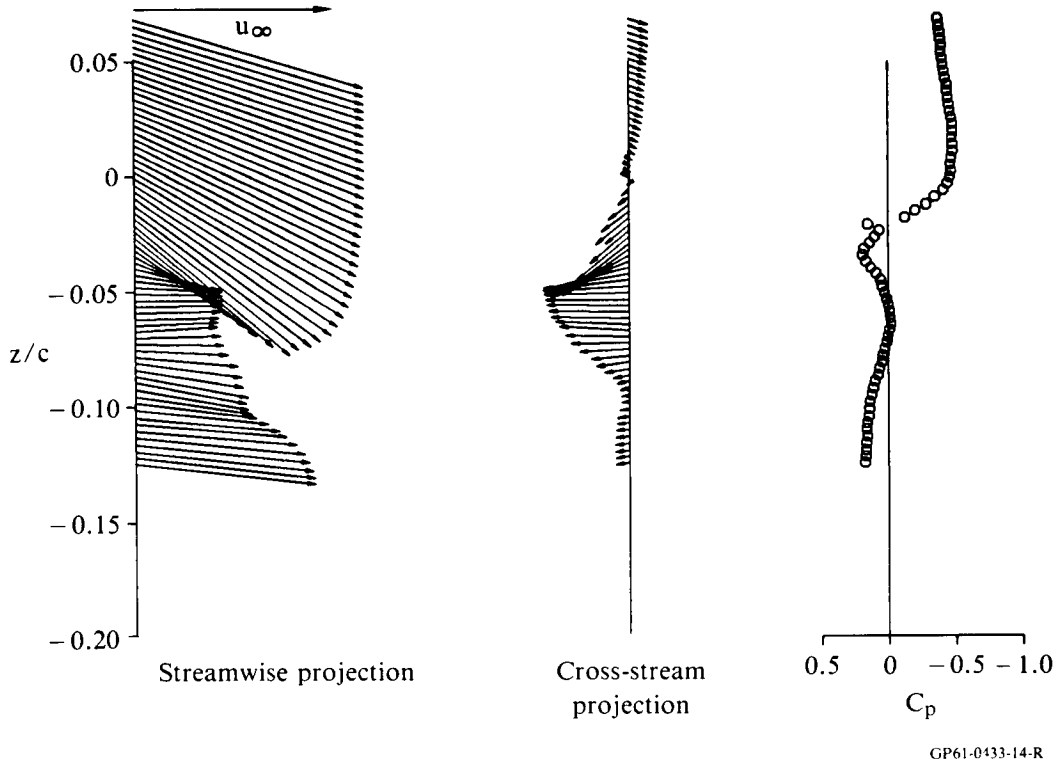

Figure 14. Wake velocity and static-pressure profiles; $M_\infty = 0.425$, $\alpha = 0°$, $p_j/p_\infty = 1.4$, $x/c = 1.02$.

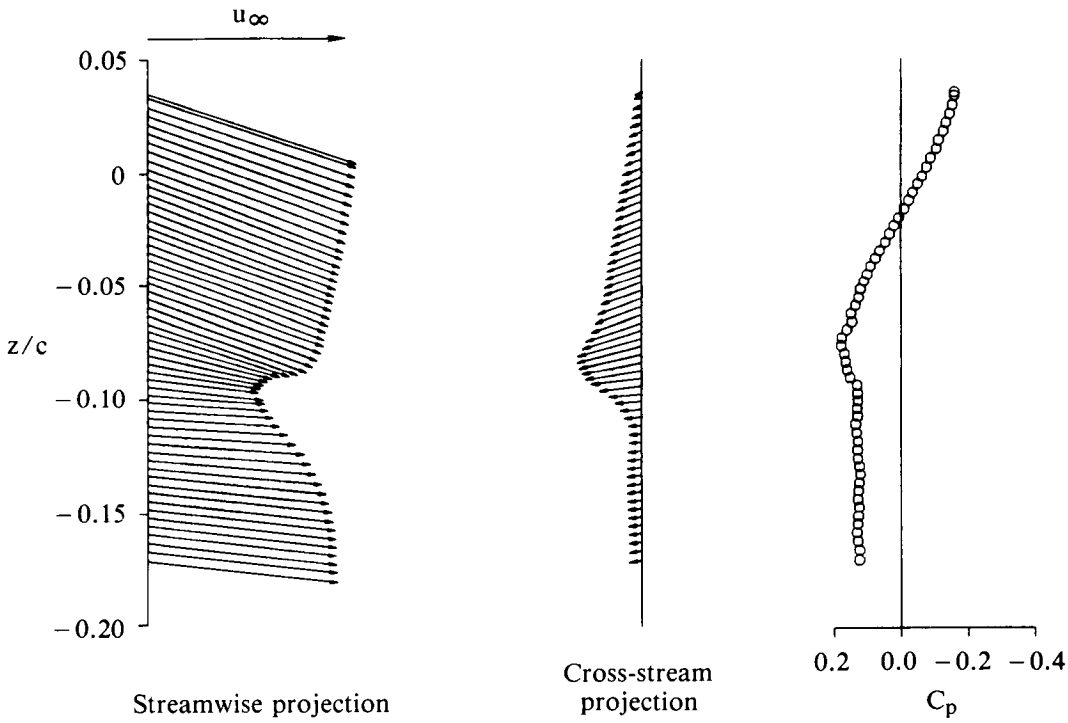

Figure 15. Wake velocity and static-pressure profiles; $M_\infty = 0.425$, $\alpha = 0°$, $p_j/p_\infty = 1.4$, $x/c = 1.10$.

The contrast between the inboard inclination of the entire profile at x/c = 0.984 and the outboard flow in the centers of the wake profiles is evident in these figures, as are the substantial variations in static pressure. As expected, the gradients decrease with increasing distance downstream.

The influence of an increase in blowing rate may be seen by comparing figures 8 and 16. The upper-surface boundary layer and wake velocities are significantly greater at the higher blowing rate, and the values of σ in the wake are more negative, resulting in a substantial region of flow outside the probe-calibration range for the innermost wake profile. These data also show large positive values of β downstream of the trailing edge. The two lower-surface boundary-layer profiles shown in figure 16 indicate that the increased blowing rate has also resulted in a forward movement of the lower-surface separation point.

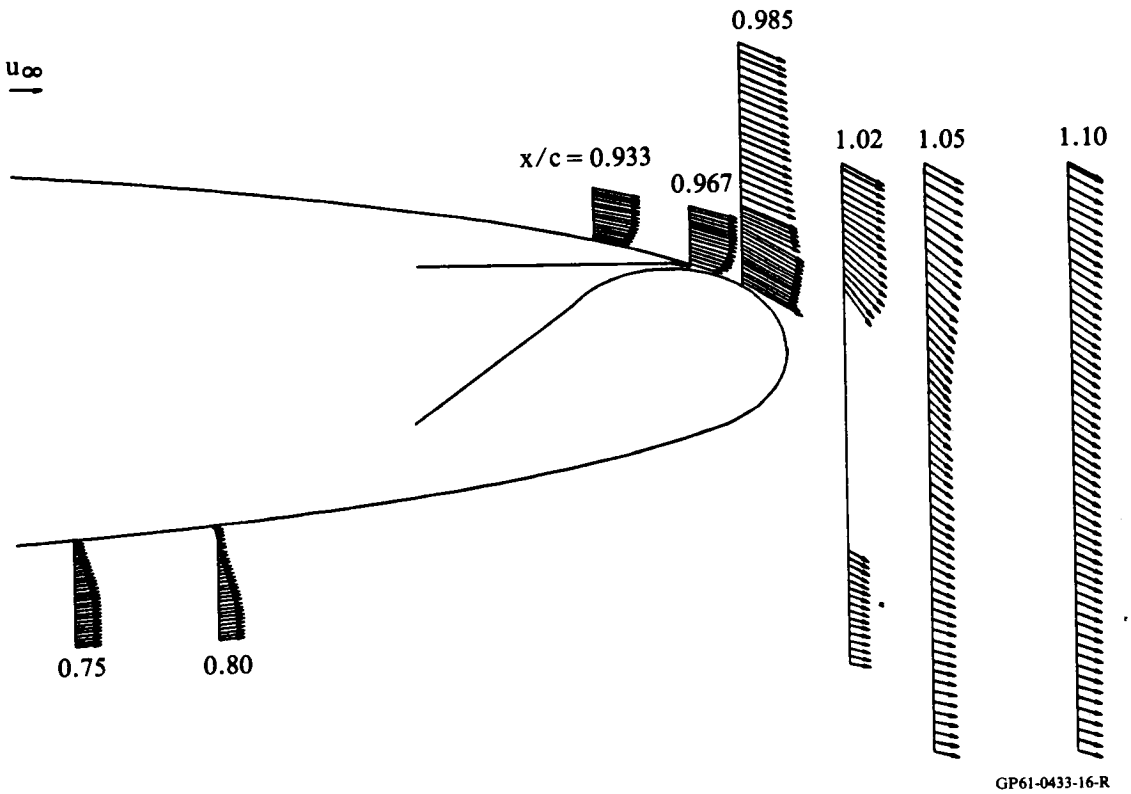

Figure 16. Velocity components in streamwise section plane; $M_\infty = 0.425$, $\alpha = 0°$, $p_j/p_\infty = 1.8$.

Figures 17-19 present close-ups of wall-jet and wake profiles for the test conditions of figure 16 in the manner of figures 13-15.

Static-pressure distributions corresponding to no blowing and three blowing rates at M_∞ = 0.70 and α = 0°, test conditions for which boundary-layer and wake data were obtained, are presented in figure 20. The data correspond to approximately the same pressure-ratio range as those of figure 6, but the values of C_μ and c_ℓ are smaller.

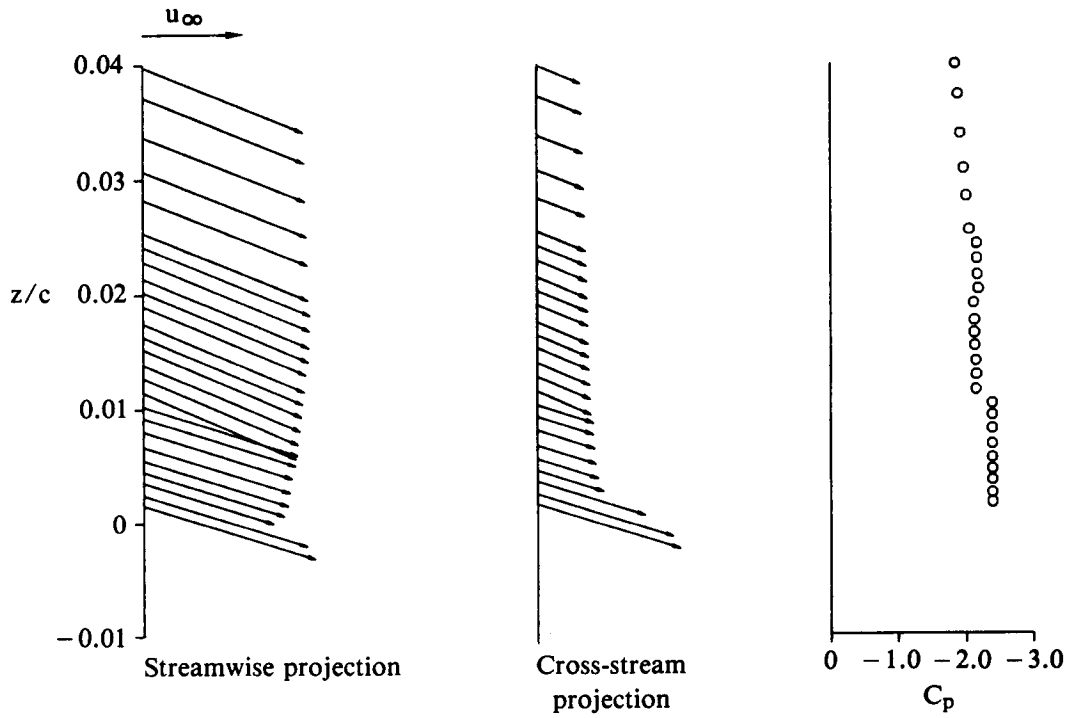

Figure 17. Wall-jet velocity and static-pressure profiles; $M_\infty = 0.425$, $\alpha = 0°$, $p_j/p_\infty = 1.8$, $x/c = 0.976$.

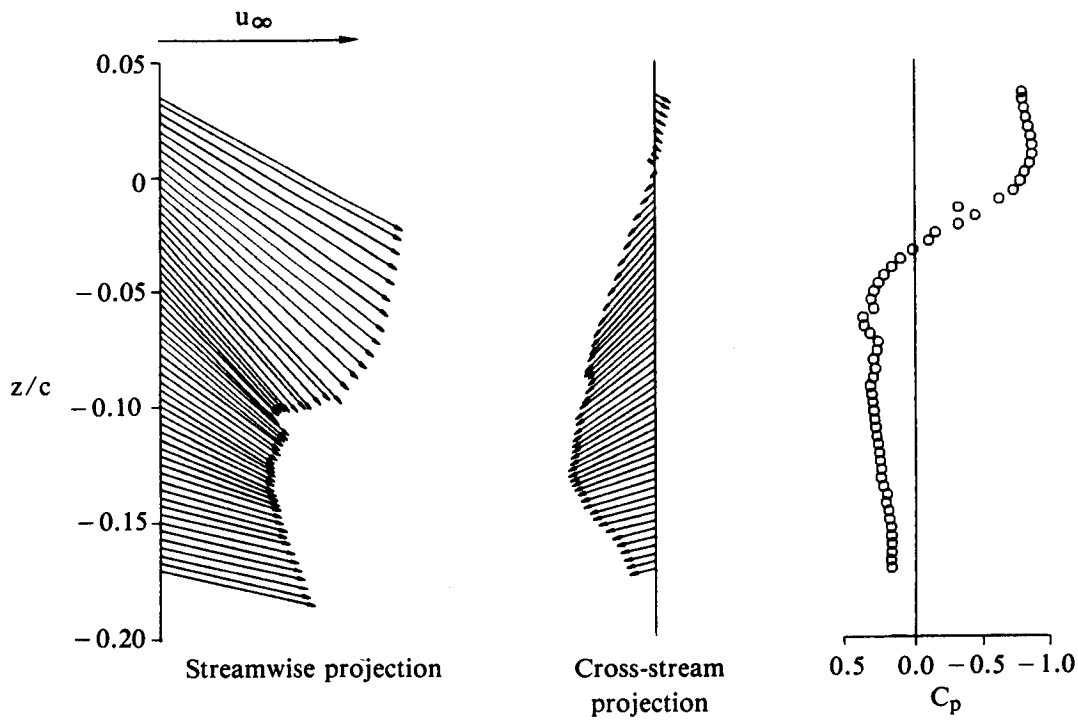

Figure 18. Wake velocity and static-pressure profiles; $M_\infty = 0.425$, $\alpha = 0°$, $p_j/p_\infty = 1.8$, $x/c = 1.05$.

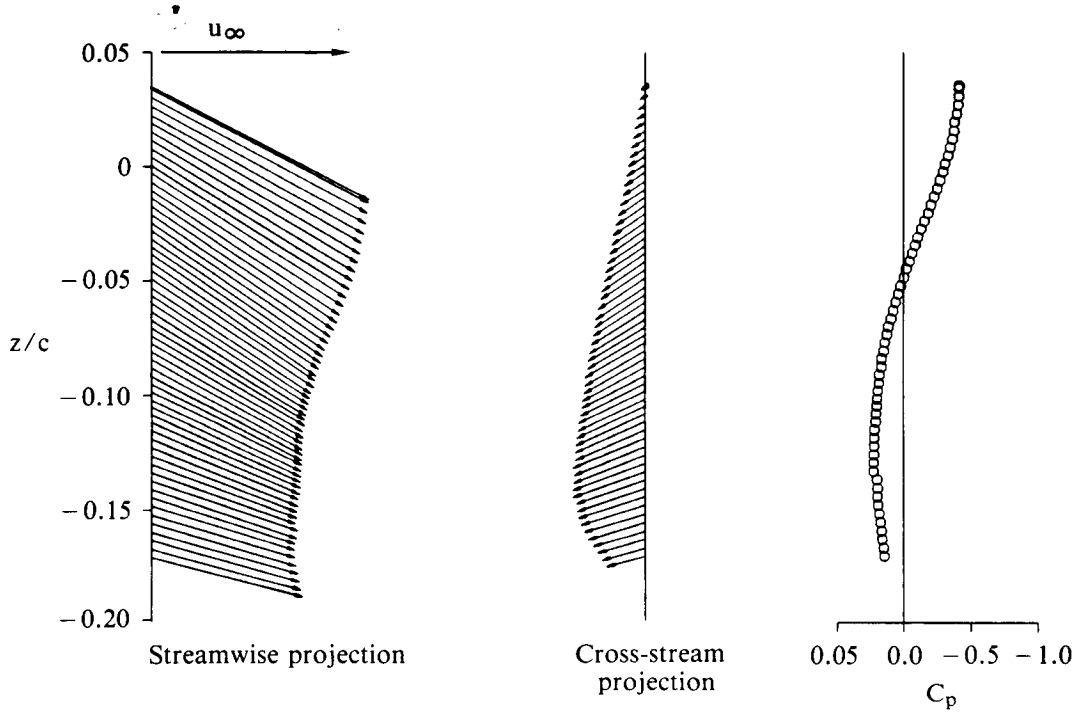

Figure 19. Wake velocity and static-pressure profiles; $M_\infty = 0.425$, $\alpha = 0°$, $p_j/p_\infty = 1.8$, $x/c = 1.10$.

GP61-0433-19-R

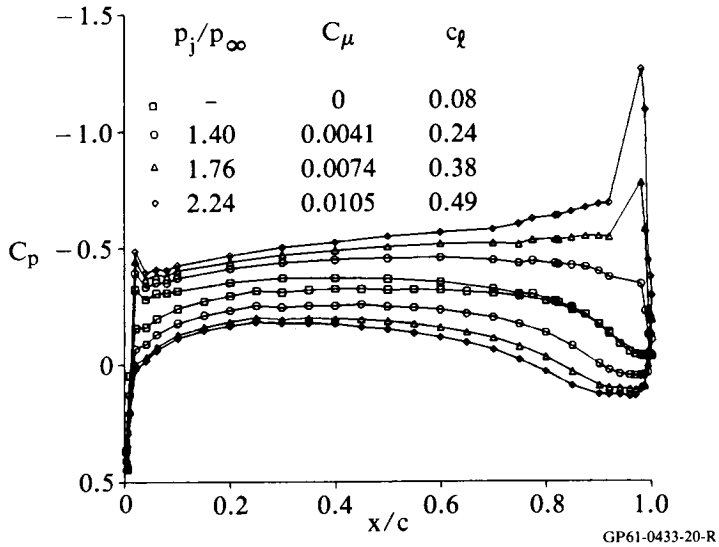

GP61-0433-20-R

Figure 20. Wing static-pressure distributions at mid-semispan; $M_\infty = 0.70$, $Re_c = 3.15 \times 10^6$, $\alpha = 0°$.

The composite view presented in figure 21, and the detailed profile data of figures 22-24, correspond to $M_\infty = 0.70$, the same jet pressure ratio as in figure 8, $p_j/p_\infty = 1.4$, but a lower jet-momentum coefficient, $C_\mu = 0.0041$. The influence of the jet on the surrounding flow is clearly much less pronounced at this test condition. The upper-surface boundary-layer profiles in the vicinity of the jet are less full and

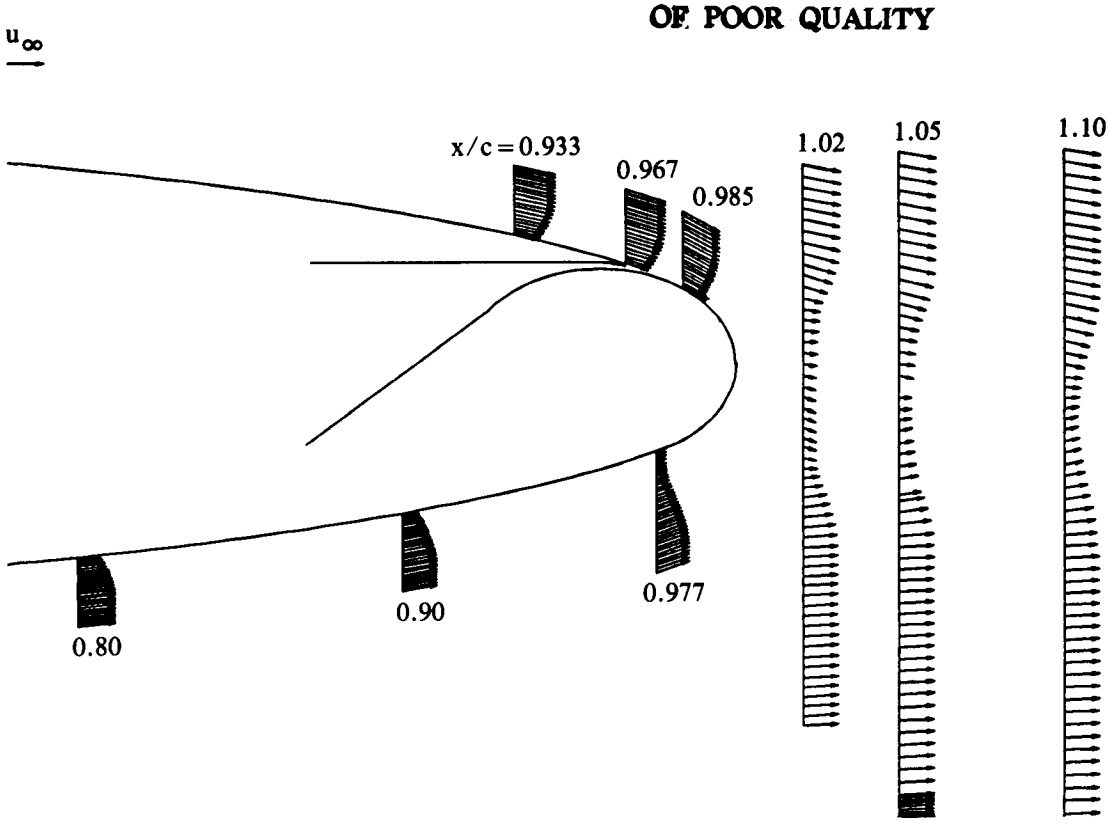

Figure 21. Velocity components in streamwise section plane; $M_\infty = 0.70$, $\alpha = 0°$, $p_j/p_\infty = 1.4$.

GP61-0433-21-R

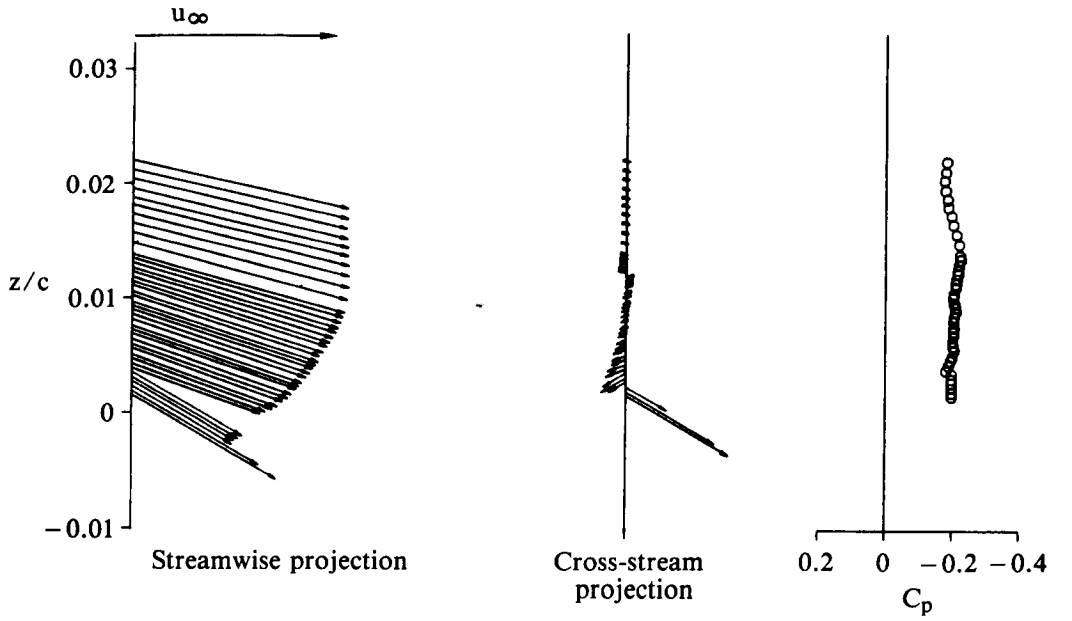

GP61-0433-22-R

Figure 22. Wall jet velocity and static-pressure profiles; $M_\infty = 0.700$, $\alpha = 0°$, $p_j/p_\infty = 1.4$, $x/c = 0.985$.

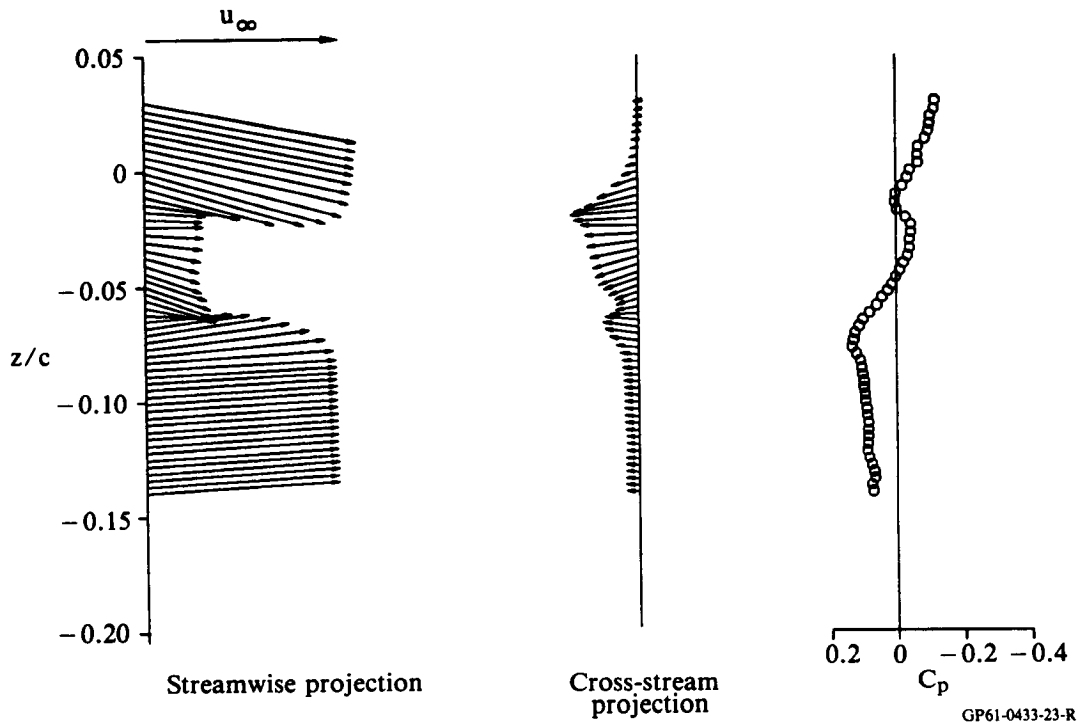

Figure 23. Wake velocity and static-pressure profiles; $M_\infty = 0.700$, $\alpha = 0°$, $p_j/p_\infty = 1.4$, $x/c = 1.02$.

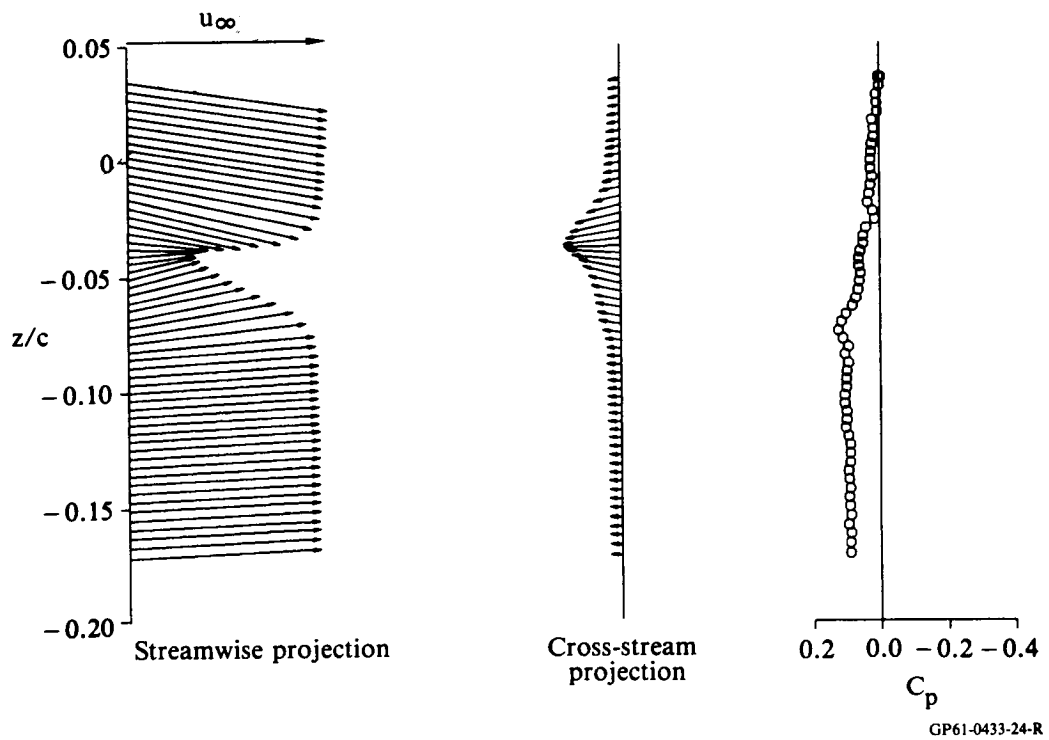

Figure 24. Wake velocity and static-pressure profiles; $M_\infty = 0.700$, $\alpha = 0°$, $p_j/p_\infty = 1.4$, $x/c = 1.1$.

show positive values of β near the surface upstream of the jet and at the location of minimum velocity in the profile downstream of the jet. The lower-surface separation line is apparently near the last measuring station on the lower surface. The reduced circulation is indicated by the reduced downward displacement of the wake centerline, relative to the data of figure 8.

Upper-surface, streamwise displacement-thickness distributions, normalized by the streamwise chord, δ_1^*/c, are presented in figure 25 for $M_\infty = 0.425$, $\alpha = 0°$, and jet conditions of no blowing, $p_j/p_\infty = 1.4$, and 1.8. The boundary-layer thickness distribution is apparently unaffected by blowing for $x/c \leq 0.5$. The displacement thickness at $x/c = 0.5$ is approximately the same as that corresponding to flow over a flat plate at the freestream conditions. In the vicinity of the slot, the displacement-thickness distribution for no blowing grows rapidly as the flow approaches separation. Data for the two blowing rates show values of displacement thickness immediately upstream of the slot which are essentially the same as those measured at mid-chord.

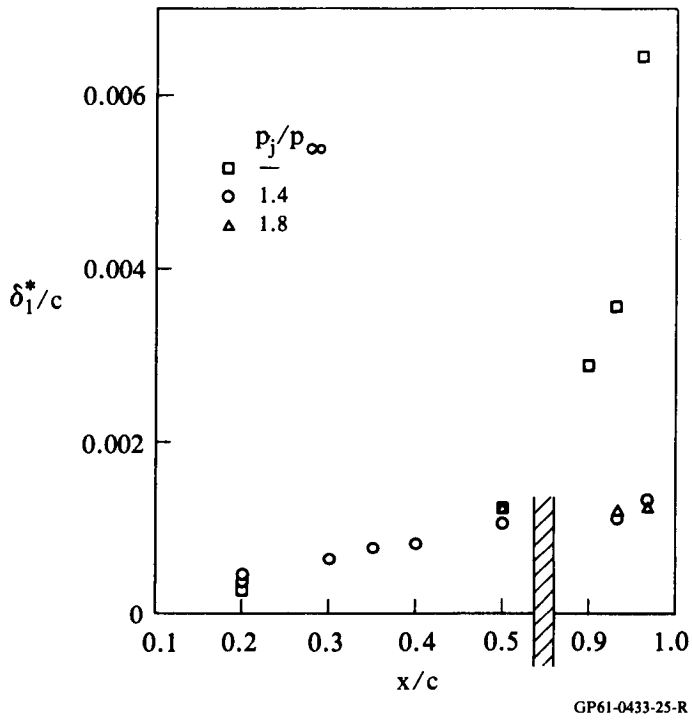

Figure 25. Upper-surface streamwise displacement-thickness distributions; $M_\infty = 0.425$, $\alpha = 0°$.

The next group of figures illustrates an abrupt transition from incipient separation at the slot location to attached flow at $M_\infty = 0.425$ and $\alpha = 5°$. Upper-surface static-pressure distributions for the relevant test conditions are shown in figure 26. Velocity-magnitude profiles at two chordwise stations downstream of the jet exit location, $x/c = 0.977$ and 0.985, are shown in figure 27 for three blowing rates. The shapes of the velocity profiles above the jet corresponding to $p_j/p_\infty = 1.2$ are characteristic of boundary layers near separation, and the minimum values of velocity measured at the interface between the wall jet and the outer flow are low, indicating min-

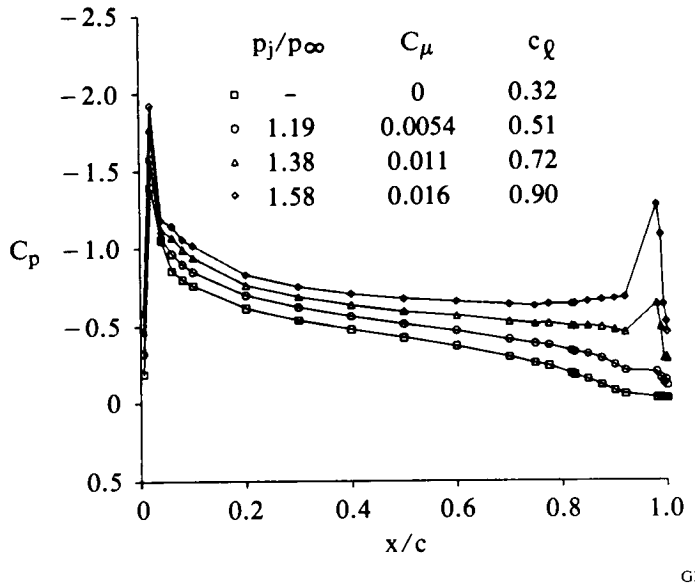

Figure 26. Upper-surface wing static-pressure distributions at mid-semispan; $M_\infty = 0.425$, $Re_c = 2.24 \times 10^6$, $\alpha = 5.0°$.

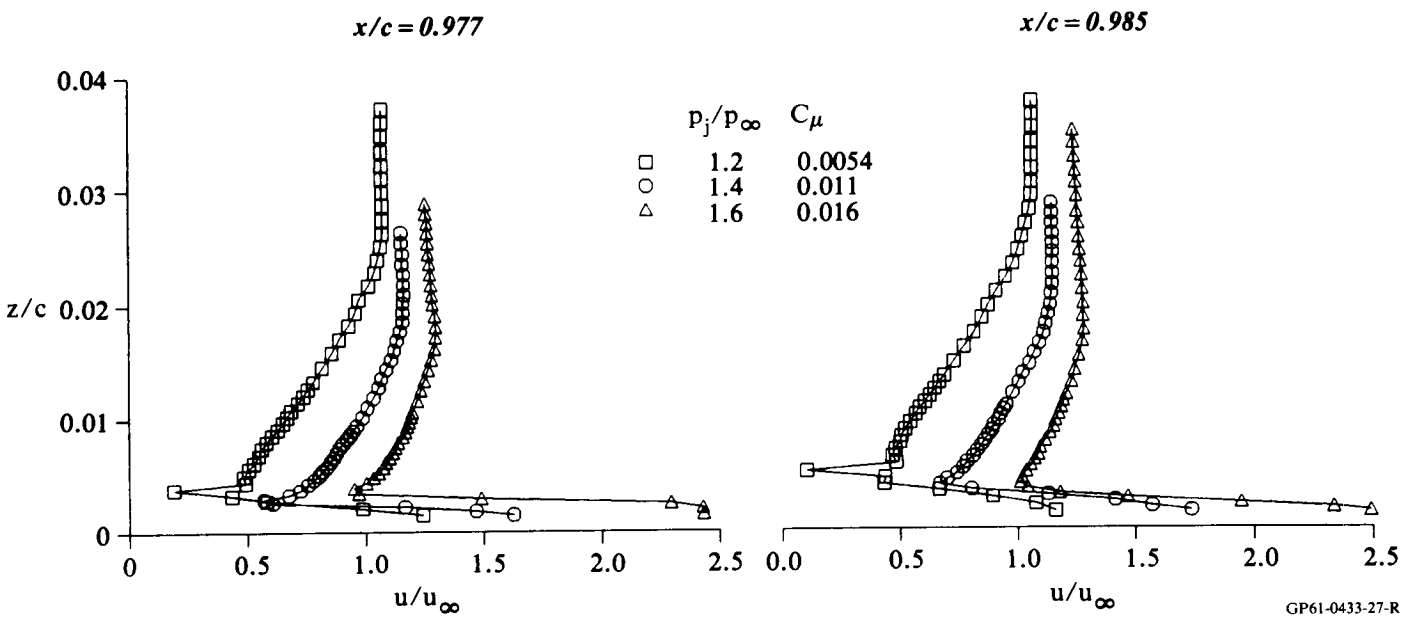

Figure 27. Velocity magnitude profiles; $M_\infty = 0.425$, $\alpha = 5°$.

imal entrainment of the outer flow by the jet. The situation for p_j/p_∞ = 1.4 is different, in that the boundary-layer portions of the profiles are relatively thin and full, and the minimum values of velocity are significantly greater. The velocity magnitudes are higher at the next higher blowing rate, p_j/p_∞ = 1.6, but the qualitative features are similar to those exhibited by the profiles corresponding to p_j/p_∞ = 1.4.

Figure 28 shows two upper-surface fluorescent oil-flow photographs corresponding to $M_\infty = 0.425$, $\alpha = 5°$, and $p_j/p_\infty = 1.2$ and 1.3, obtained from Keener et al., (1986). The oil was injected from surface orifices and photographed during a run. At the lower blowing rate, the oil streaks turn toward the spanwise direction near the slot, indicating separation at the slot, except in the immediate vicinity of the tip. The pattern obtained for $p_j/p_\infty = 1.3$ is significantly different, showing streamwise flow along the span up to the slot, indicating attached flow at the slot.

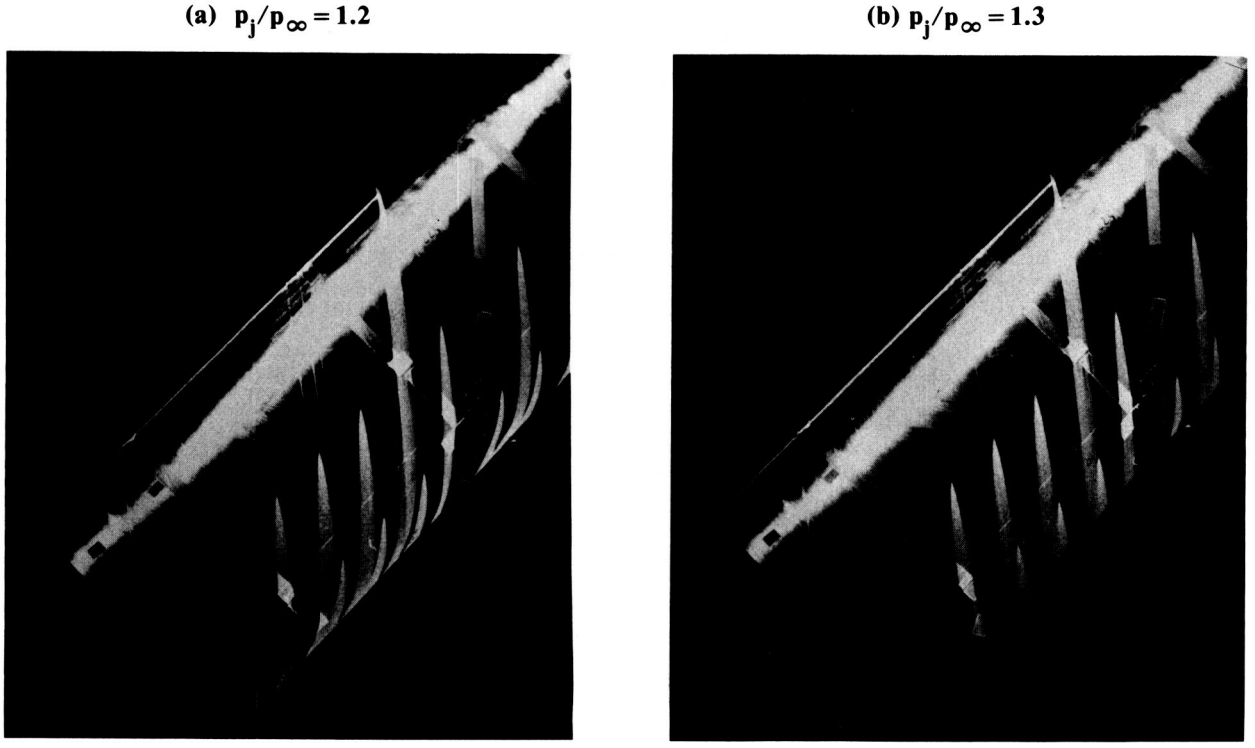

Figure 28. Fluorescent oil-flow photographs of wing upper surface; $M_\infty = 0.425$, $\alpha = 5°$.

Data at $M_\infty = 0.70$ and $\alpha = 5°$ were examined for evidence of similar behavior. Upper-surface static-pressure distributions corresponding to this Mach number and angle of attack for which flowfield survey data were obtained are shown in figure 29. Wall-jet profiles at x/c = 0.977, having the most nearly similar characteristics to those of figure 27, are shown in figure 30, corresponding to $p_j/p_\infty = 1.6$ and 2.0. However, the oil-flow photograph of figure 31, obtained at conditions corresponding to the higher-blowing-rate data of figure 30, indicates flow separation at the slot.

Values of skin-friction coefficient, C_f, were determined from the attached boundary-layer profiles by fitting the inner region of the velocity magnitude profiles to the following generally accepted similarity law,

$$\frac{u}{u_\tau} = \frac{1}{0.41} \ln\left(\frac{z u_\tau}{\nu}\right) + 5.0 \qquad (1)$$

where u_τ is the shear velocity, $\sqrt{\tau_w/\rho}$; τ_w is the wall shear stress, ρ is the density, and ν is the kinematic viscosity. A range of values has been proposed for the con-

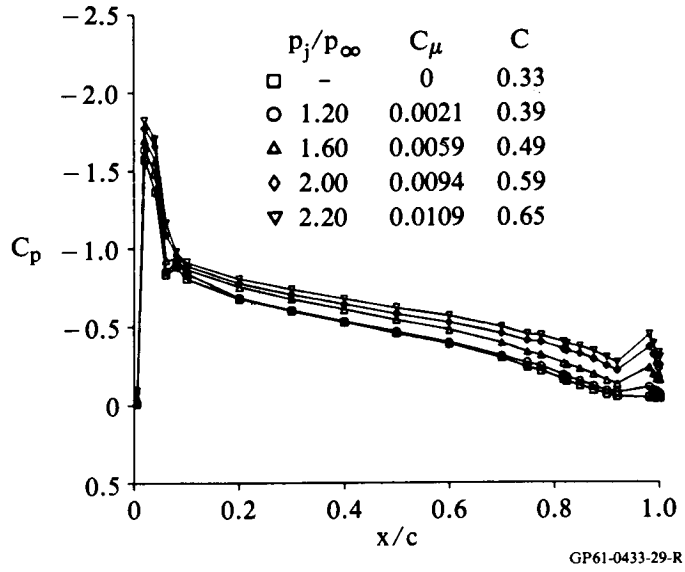

Figure 29. Upper-surface wing-static-pressure distributions at mid-semispan; $M_\infty = 0.70$, $Re_c = 3.15 \times 10^6$, $\alpha = 5°$.

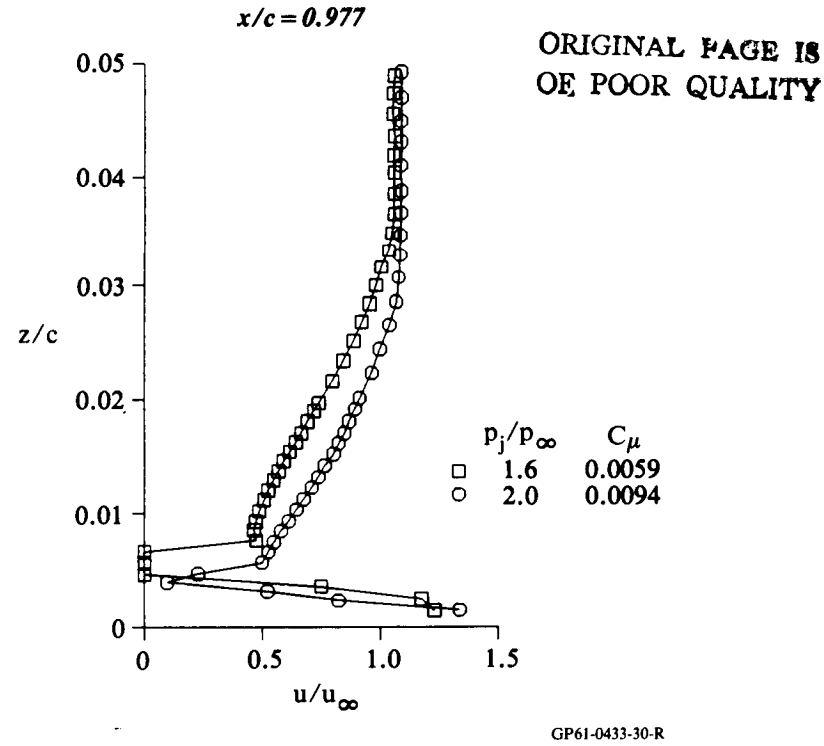

Figure 30. Velocity magnitude profiles; $M_\infty = 0.700$, $\alpha = 5°$.

ORIGINAL PAGE IS
OF POOR QUALITY

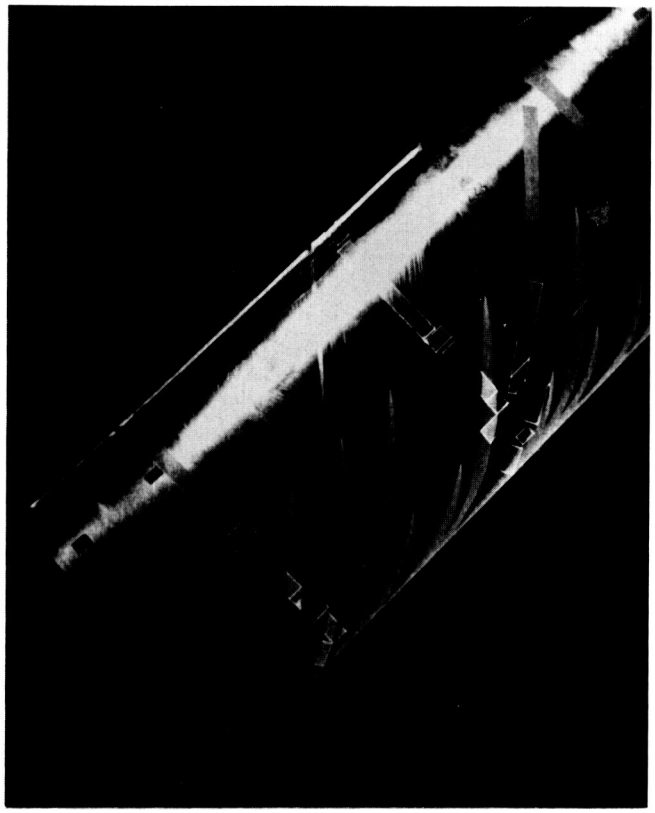

GP61-0433-31-R

Figure 31. Fluorescent oil-flow photograph; $M_\infty = 0.7$, $\alpha = 5°$, $p_j/p_\infty = 2.0$.

stants in this equation; this situation is reviewed by Pierce et al. (1982,1). Extension of the incompressible law-of-the-wall to flows with moderate compressibility effects is usually accomplished by evaluating the density and viscosity at the wall temperature. Prahlad (1968) proposed that this similarity law be extended to three-dimensional flows by replacing the two-dimensional velocity in equation (1) with the velocity magnitude. Pierce et al. (1982,2) concluded that the magnitude of the wall shear stress could be determined by the Clauser-chart technique (Clauser, 1954) to within 5-10% if data in the range $10 \leq z^+ \leq 100$ ($z^+ = zu_\tau/\nu_w$) were used. This conclusion was limited to monotonically-skewed boundary layers with an approximate maximum of 15-20° of skew. The attached boundary-layer profiles of figures 7 and 8 are nearly colinear, and are representative of the attached profiles measured in this investigation. It is concluded that the Clauser-chart technique should be adequate for estimating skin-friction magnitudes from the present data.

Figure 32 illustrates the method by which this technique was applied to the present data. Lower-surface velocity-magnitude profiles corresponding to the baseline test conditions are plotted in semi-logarithmic coordinates. In these coordinates, equation (1) represents a family of straight lines with C_f as a parameter. Since the straight lines in figure 32 represent the range $10 \leq zu_\tau/\nu \leq 1000$, it is apparent that the sublayer and the inner portion of the logarithmic region are not resolved in these data. The data show a monotonically decreasing trend of C_f with x/c.

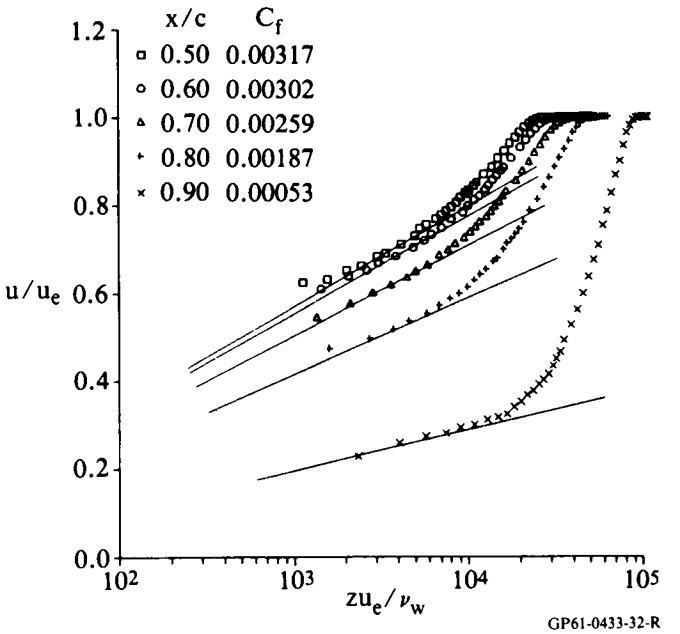

Figure 32. Lower-surface velocity magnitude profiles in semi-log coordinates; $M_\infty = 0.425$, $\alpha = 0°$, $p_j/p_\infty = 1.4$

The influence of blowing rate on the position of the lower-surface separation line is shown in figure 33, in which C_f is plotted as a function of x/c for a range of blowing rates. It is assumed that extrapolation of values of C_f to zero provides a reasonable estimate of the separation-line location. (Actually, the velocity magnitudes become small and the local flow direction becomes parallel to the wing generators near separation.) It is shown that the separation line moves upstream with increasing blowing rate, up to $p_j/p_\infty = 1.8$, but an additional increase of p_j/p_∞ to 2.2 does not produce an additional forward movement of the separation line. It is in this range of blowing rates that the performance data (c_ℓ versus C_μ) show no additional increase of lift with increasing blowing rate.

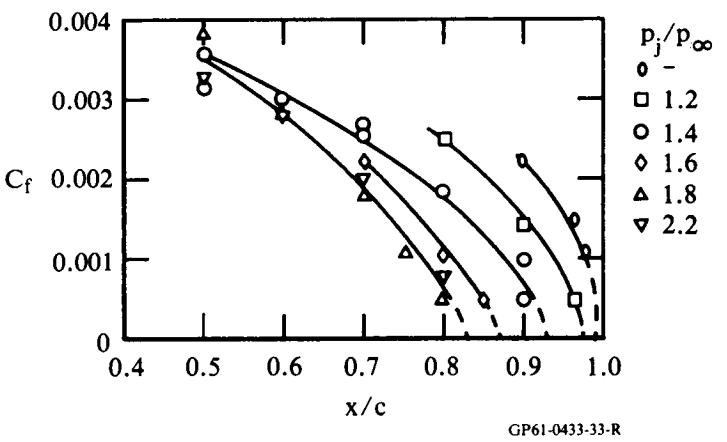

Figure 33. Lower-surface skin-friction distributions; $M_\infty = 0.425$, $\alpha = 0°$.

Streamwise displacement-thickness data corresponding to the skin-friction data of figure 33 are presented in figure 34, where the approach to separation is indicated by a rapid growth in displacement thickness with increasing downstream distance. Vertical dashed lines in figure 34 indicate the separation locations inferred from the skin-friction data.

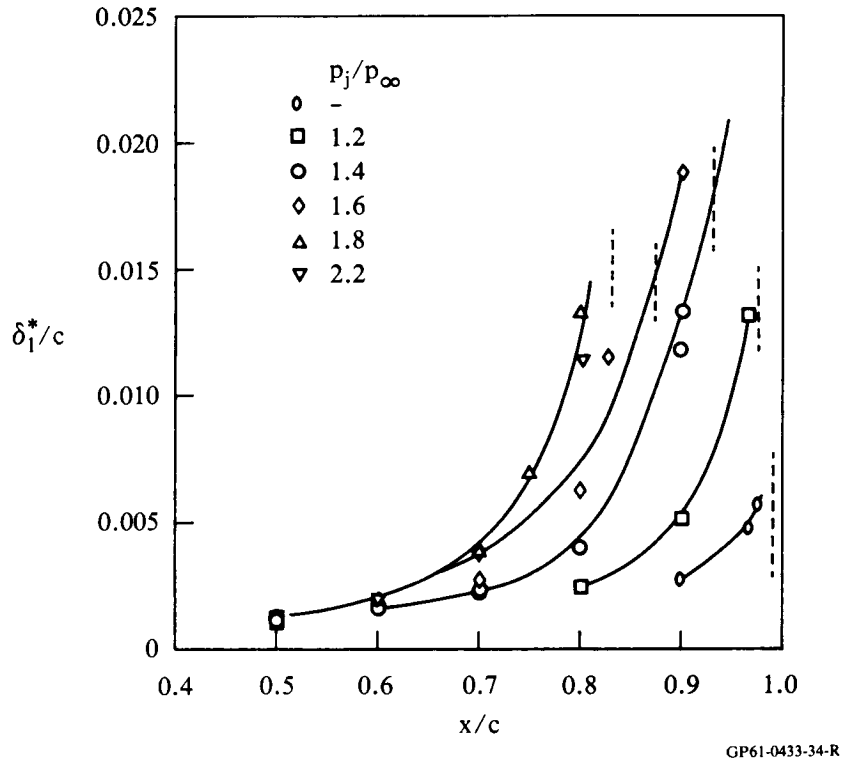

Figure 34. Lower-surface streamwise displacement-thickness distributions; $M_\infty = 0.425$, $\alpha = 0°$.

CONCLUDING REMARKS

Boundary-layer and wake-survey data were obtained at mid-semispan in the flow about a 45° swept, circulation-control wing at freestream Mach numbers of 0.425 and 0.70. Boundary-layer profiles forward on the wing on both upper and lower surfaces are approximately streamwise and two-dimensional. The flow in the vicinity of the jet exit and in the near wake is highly three-dimensional. Qualitative variations in flowfield features with freestream Mach number and jet blowing rate are illustrated by velocity vector plots. The jet flow near the slot on the Coanda surface is directed normal to the slot, or 45° inboard. All near-wake surveys, including surveys obtained 1% chord downstream of the trailing edge, show large outboard flows at the center of the wake. At Mach 0.425 and 5° angle of attack, a range of jet blowing rates was found for which an abrupt transition from incipient separation to attached flow occurs in the boundary layer upstream of the slot. The variation in the lower-surface separation location with blowing rate was determined from boundary-layer measurements at Mach 0.425.

REFERENCES

Clauser, F. H.: Turbulent Boundary Layers in Adverse Pressure Gradients, J. Aero. Sci., vol. 21, no. 2, Feb. 1954, pp. 91-108.

Dudzinski, Thomas J.; and Krause, Lloyd N.: Flow-Direction Measurement with Fixed-Position Probes. NASA TM X-1904, 1969.

Keener, Earl R.; Sanderfer, Dwight T.; and Wood, Norman J.: Pressure Distributions and Oil-Flow Patterns for a Swept Circulation-Control Wing. NASA CP-2432, 1986. (Paper 10 of this compilation.)

Pierce, F. J.; McAllister, J. E.; and Tennant, M. H.: Near-Wall Similarity in Three-Dimensional Turbulent Boundary Layers, Part I: Model Review. **Three-Dimensional Turbulent Shear Flows**, American Society of Mechanical Engineers, New York, 1982, pp. 85-95.

Pierce, F. J; McAllister, J.E.; and Tennant, M. H.: Near-Wall Similarity in Three-Dimensional Turbulent Boundary Layers, Part II: Pressure-Driven Flow Results. **Three-Dimensional Turbulent Shear Flows**, The American Society of Mechanical Engineers, New York, 1982, pp. 96-103.

Prahlad, T. S.: Wall Similarity in Three-Dimensional Turbulent Boundary Layers. AIAA J., vol. 6. no. 9, Sept. 1968, pp. 1772-1774.

Wood, Norman, J.; and Conlon, John A.: The Performance of a Circulation Control Airfoil at Transonic Speeds. AIAA Paper No. 83-0083, Jan. 1983.

Wood, Norman J.; and Nielsen, Jack N.: Circulation Control Airfoils Past, Present, Future. AIAA Paper No. 85-0204, Jan. 1985.

Wood, Norman J.; and Sanderfer, Dwight T.: Transonic Performance of Two Circulation Control Airfoils. NASA TM X-86767, 1987.